Physics – Uspekhi **64** (6) 535 – 557 (2021)

REVIEWS OF TOPICAL PROBLEMS PACS numbers: 07.20.Pe, **44.10.+i**, 65.80.Ck, 72.20.Pa, 73.40.Ns

Thermoelectric effect and a thermoelectric generator based on carbon nanostructures: achievements and prospects

E D Eidelman

DOI: https://doi.org/10.3367/UFNe.2020.06.038795

Contents

1. **Introduction. Uniqueness of carbon nanostructures** **535**
2. **Thermal emf in carbon nanostructures. Mechanism of ballistic phonon drag of electrons** **538**
   2.1 Qualitative picture of ballistic phonon drag of electrons; 2.2 Quantitative theory of ballistic phonon drag of electrons
3. **Thermoelectric generator based on film carbon nanostructures** **541**
4. **Thermal conduction in carbon nanostructures. Mechanism of heat transfer through the sp^2/sp^3 hybridization region interface of carbon atoms** **544**
   4.1 Qualitative picture of heat transfer through the sp^2/sp^3 region interface; 4.2 Quantitative theory of heat transfer through the sp^2/sp^3 region interface
5. **Thermoelectric generator based on a composite of an sp^2 matrix structure with diamond nanoparticles** **549**
6. **Thermal emf of graphene** **550**
   6.1 Phonon drag of electrons in graphene; 6.2 Calculation of the thermal emf coefficient in graphene
7. **Thermoelectric generator based on an sp^2 region graphene matrix composite** **553**
8. **Conclusions. Path to a thermoelectric generator with record parameters** **554**
   References **555**

Abstract. Graphite-like (metal!) regions and diamond-like (dielectric!) regions in carbon nanostructures are very closely spaced. Based on this unique feature, a model of thermal emf produced due to the drag of electrons by ballistic phonons is developed and a model of thermal conduction during heat transfer through the graphite-like/diamond-like region interface is proposed. Experiments with a thermoelectric generator based on film carbon nanostructures are analyzed. Models of a thermoelectric generator based on a composite of a graphite-like matrix containing diamond nanoparticles and graphene impurities are proposed. These models both demonstrate the above-mentioned phenomena and predict the achievement of the maximum thermoelectric conversion efficiency.

Keywords: thermoelectric generator, electron–phonon interaction, carbon nanostructures, ballistic phonon drag of electrons, graphite-like region, diamond-like region, heat transfer through the graphite-like/diamond-like region interface, composite of a graphite-like matrix with inclusions of diamond nanoparticles, graphene, thermoelectric generator efficiency

E D Eidelman
Ioffe Institute, ul. Politekhnicheskaya 26, 194021 St. Petersburg, Russian Federation;
St. Petersburg State Chemical-Pharmaceutical University, ul. Prof. Popova 14, 197376 St. Petersburg, Russian Federation;
Peter the Great St. Petersburg Polytechnic University, ul. Politekhnicheskaya 29, 195251 St. Petersburg, Russian Federation
E-mail: Eidelman@mail.ioffe.ru

Received 19 April 2020, revised 26 May 2020
Uspekhi Fizicheskikh Nauk **191** (6) 561 – 585 (2021)
Translated by M Sapozhnikov

1. Introduction. Uniqueness of carbon nanostructures

A distinct feature of carbon is the existence of two basic allotropic forms (Fig. 1). One of them, graphite (Figs 2a, b) with atoms with the sp^2 hybridization of electrons (Fig. 1a), is characterized by semimetal properties, has comparatively low heat conduction and heat capacity, but contains free charge carriers. The other allotropic form, diamond (Figs 2c, d) with atoms with the sp^3 hybridization (Fig. 1b), has high heat conduction and heat capacity and is a wideband semiconductor, in fact a dielectric, and does not contain free charge carriers.

Regions with such contrasting physical properties in carbon nanostructures are located extremely close to each other (spaced less than 1 nm apart). This gives rise to the

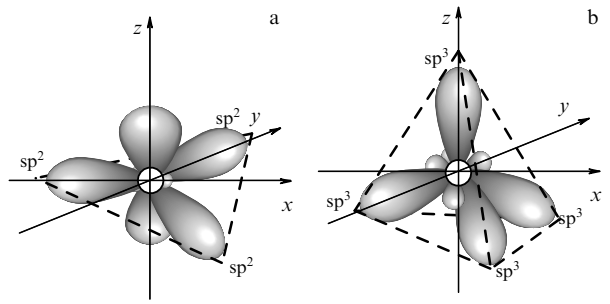

Figure 1. Carbon structures. Two types of hybridization of a carbon atom. (a) sp^2: three orbitals in a plane, (b) sp^3: four orbitals from the tetrahedron center and its top.

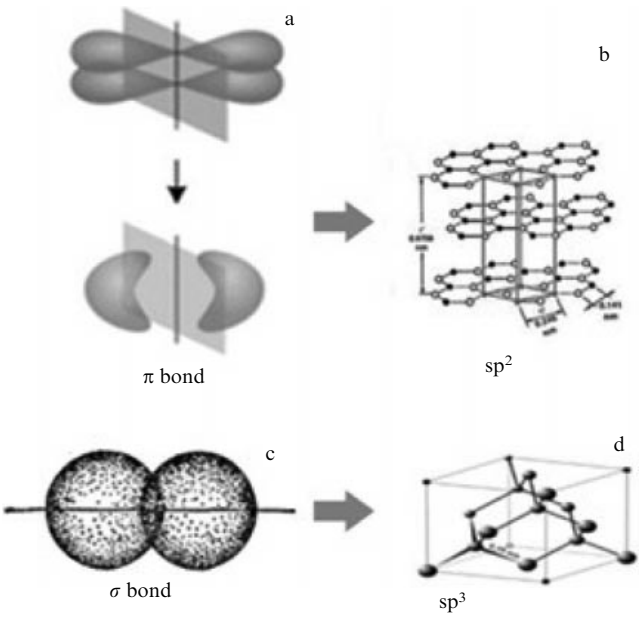

Figure 2. Carbon structures. Covalent bonds. (a) π bond corresponding to (b) the sp^2 hybridization, graphite-like structures; (c) σ bond corresponding to (d) sp^3 hybridization, diamond-like structures.

unique characteristics of electron–phonon interaction in carbon nanostructures. In such structures, regions with metal and dielectric physical properties are very closely spaced. The importance of this circumstance for creating thermoelectric elements can be compared with the important unique property of the uranium 235 isotope to produce via fission more than one neutron in nuclear fission reactors.

In regions close to the interfaces of regions with different allotropic states of carbon atoms, the ballistic transfer of phonons mainly occurs in one direction. The phonon flow in a semimetal, a graphite-like region, produces a peculiar thermoelectric effect, so-called 'phonon drag' or 'phonon wind' [1]. This effect was discovered in 1944 by my teacher L E Gurevich [2]. The efficiency of this mechanism in sp^2-sp^3 structures is 10–100 times higher than that of the usual diffusion mechanism.

After Gurevich's paper, the phonon drag concept became widely applied (see, e.g., monographs [3, 4]). In [5, 6], more general equations were used in which the drag transfer was compared with the diffusion process. In [5], the equation specifying both these effects was analyzed, and this equation was compared with the Fourier equation for the case of heat transfer in a thin film perpendicular to its layer. It was shown that the equation specifying both the drag and diffusion much better approximates solutions of the kinetic equation than the Fourier equation. However, to obtain the qualitative results presented in this review, the use of these more complicated equations is not required (see Sections 2 and 4).

Another characteristic inherent in carbon nanostructures explained by the unique close spacing of regions with metal and dielectric physical properties is high thermal boundary resistance — the Kapitza resistance. The general problem of interfacial heat transfer is relevant in both theoretical and experimental physics, because this phenomenon is often encountered in technical applications: the sp^2/sp^3 region interface corresponds to the metal/dielectric interface. Electrons cannot pass from the sp^2 region (semimetal) to the sp^3 region (dielectric); they cannot overcome the sp^2/sp^3 interface, and heat is transferred through the interface only by the phonon flow. Therefore, temperature drops mainly appear at the sp^2/sp^3 interface [7].

The thermal resistance in nanostructures is well studied [8–20]. Metal/metal or dielectric/dielectric pairs have been investigated. Studies of thermal resistance at the metal/dielectric interfaces in carbon nanostructures will be considered at the beginning of Section 4. As for the influence of contacting boundaries on the thermal resistance [21–32], this influence at the present stage of studies of carbon nanostructures cannot change the qualitative results and therefore is not discussed below.

All carbon nanostructures can be considered composites representing a mixture of the sp^2 and sp^3 regions.

Nanocomposites are used for various applications: as thermal interfaces, thermal-insulation materials, and materials for a new generation of solar elements or thermal cells and other thermoelectric devices [33–46].

At present, a great number of nanocomposites are being investigated. They include nanocomposites containing spherical or quasi-spherical nanoparticles in matrices (for example, Si–Ge systems in which both materials can be either a matrix or a filler); multiphase nanocomposites (for example, new thermoelectric nanomaterials: Bi_2Te_3, PbTe alloys, and SiGe nanocomposites); nanocomposites based on matrix media (polymers, solids, etc.) and nanotubes (single-wall, multiwall, straight, and bent); and nanofibers with different compositions. Complex composites are also being studied which represent a branched network of nanoinclusions (nanotubes and nanofibers bound in bundles and pellets, aggregates or networks of nanoparticles of different compositions) in polymers, nonmetal or metal matrices, and nanocomposites containing nanowires, including hollow ones [21–24].

The not simple structure of many nanocomposites, the possibility of the coexistence of phases with different sizes and physical properties, including semiconducting, metal, and dielectric phases, and the complexity of phase interfaces require consideration of the thermal properties of nanocomposites to understand the heat transfer processes in them.

In this review, we consider almost exclusively film structures. One-dimensional structures (see, e.g., [47]) and structures with superlattices [48–51] are not considered, because they are absent in carbon nanostructures. On the other hand, film materials with a high thermal electromotive force (emf) not made of carbon nanostructures but of standard semiconductors and semimetals have been extensively studied [52–63]. The thermal [64] and thermoelectric properties [65–75] of thin films made of various noncarbon materials have been investigated in detail.

A peculiar carbon structure is graphene. The propagation of heat in graphene is well studied (see, e.g., [76–80]). As for the thermoelectric properties of graphene, a few studies in this field are presented in Section 6.

In this review, the properties of carbon nanotubes and fullerenes are not considered. It is difficult to call them nanostructures; most likely they can be treated as polymers.

One of the most important applications of nanothermal physics is the study and use of thermoelectricity observed in some nanostructures. Undoubtedly, we will see in the nearest future intense development of new avenues in energetics and cooling systems. The design of thermoelectric generators (TEGs) based on semiconductor and semimetal films has

already been studied in many papers [81–92]. General concepts of TEGs are considered in numerous books and reviews [93–107], and therefore they are not discussed here. Most attention is directed to investigations of thermoelectric phenomena in nanostructured systems and materials. These structures include carbon film nanostructures, composites of carbon nanostructures, and graphene. All the results obtained in investigations of TEGs based on conventional materials are used, of course, in the development of TEGs based on carbon nanostructures. Below, our attention will be focused on the new features introduced into the thermoelectric effect by the carbon nanostructure.

The aim of this review is to show how the drag and thermal resistance phenomena observed in carbon nanostructures can be used to achieve record thermoelectric parameters and to develop scientific foundations and TEG constructions operating based on these mechanisms.

In the review, a fundamentally new approach to the TEG structure and materials is discussed, which provides, as follows from theoretical estimates, the maximum thermoelectric conversion. The TEG designs and materials proposed here are protected with Russian patents [108–110]. Theoretical estimates presented below confirm the correctness of the approach chosen. The experimental verification of the approaches proposed is discussed and the solution to the key problem of a substantial increase in TEG efficiency is considered.

We were the first to focus in 2004 on the unique properties of a carbon nanostructure [111]. Recent studies have allowed us to move to the practical realization of new ideas. This was facilitated by an RSF project headed by the author in 2016–2018.

At present, there is a method for preparing monodisperse sols of diamond nanoparticles about 5 nm in size [112, 113], and monoatomic graphene layers were prepared from thermally expanded graphite and studied in [114, 115].

The task of this review is to attract attention to the verification of fundamentally new scientific ideas, which can provide, in our opinion, a significant increase in the efficiency of thermoelectric generators.

It is known (see, e.g., [116]) that the TEG efficiency is determined by the quality parameter $Z = \gamma^2\sigma/\chi$, where γ is the thermoelectric power or the Seebeck coefficient, and σ and χ are the electric conduction and heat conduction coefficients, respectively. The main problems in the choice of a thermoelectric functional material are to increase γ and decrease χ without a simultaneous increase in σ. Unfortunately, the heat conduction and electric conduction are usually proportional to each other, following the known Wiedemann–Franz law (see, e.g., [117]). In the best TEGs existing at present, $ZT = 1.5$ at room temperature [118, 119].

It was shown in [120] that the electronic efficiency of thermoelectric generation can approach the thermodynamic Carnot limit if the electron transfer between hot and cold reservoirs occurs at one energy level for the finite temperature gradient and finite external potential difference. This takes place in the absence of phonon heat conduction and thermal losses.

This result shows that in principle it is possible to approach the Carnot limit in thermoelectric devices in the case of large ZT. It is possible to obtain the maximum electric current and energy flux by reducing at the same time the heat conduction [121–124]. This means violating the Wiedemann–Franz law relating the electric and heat conductions.

In this review, only the Seebeck effect is considered. The application of the results to other thermoelectric and thermal effects in carbon nanostructures is obvious.

The first new idea discussed below is the increase in the thermal emf coefficient γ using the electron drag produced by a thermal flow of noncolliding ballistic phonons. The second one is the reduction in the heat conduction coefficient χ due to heat (phonon) scattering by the sp^2/sp^3 metal/dielectric interface in a composite when a directly proportional relation between the heat conduction χ and electric conduction σ is absent.

The laboratory TEG model (patent [109]), developed to realize the first idea, consists of alternating layers with the sp^2 and sp^3 hybridized electron shells of carbon atoms (see Sections 2 and 3). The thermal emf of such a TEG is mainly determined not by usual diffusion, but by an order of magnitude more efficient process of electron drag by a thermal flow of ballistic phonons. The laboratory TEG model (patent [108]), developed to realize simultaneously both ideas, is a composite containing diamond-like particles embedded into a matrix made of a graphite-like material. The scattering of heat by sp^2/sp^3 interfaces in such a composite considerably reduces the heat conduction, and electron drag by ballistic phonons occurs.

In Sections 4 and 5, some models describing heat transfer in various situations are presented, and we analyze studies of the heat conduction of composites containing a matrix with sp^2 hybridized carbon atoms doped with detonation synthesis diamond nanoparticles 4–5 nm in size. Such composites were shown to be the most promising for creating thermoelectric generators with record parameters.

The creation of such a structure seemed impossible even only a few years ago. The main obstacle in the way of developing a TEG based on carbon nanostructures is the difficulty preparing a sharp enough interface layer between an artificially deposited carbon film with the sp^2 hybridized electron shells of atoms and a film with the sp^3 hybridization. Hopefully, this problem can be solved using a new technological achievement — the microwave plasma chemical vapor deposition (MWPCVD) method capable of providing the interface thickness closest to the required value [125, 126].

The technological experience in the preparation of sp^2 and sp^3 hybridization structures by the chemical vapor deposition (CVD) method also seems promising for the development of TEGs [125, 127]. Progress in the growing of carbon nanostructures by the CVD method, the development of methods for controlling parameters of layers at the atomic level, experience in the development of technology, and studies of diamond nanoparticles and graphene have provided the beginning of practical realization of these new ideas.

Three types of sp^2-sp^3 structures are discussed in the review.

(1) The two-layer sp^2-sp^3 structure in which the sp^2 layer no more than 50–20 nm in thickness is adjacent to the sp^3 layer more than an order of magnitude thicker. This structure should be prepared in one technological cycle (see Section 3).

(2) The two-layer composite–sp^3 structure in which the composite is an sp^2 matrix containing diamond nanoparticles with the sp^3 hybridization. The composite layer 50–20 nm and smaller in thickness is adjacent, as in structure (1), to the sp^3 layer an order of magnitude thicker than the composite layer (see Section 5).

(3) The two-layer composite–sp^3 structure in which the composite is an sp^2 matrix containing graphene. The

composite layer 50–20 nm and smaller in thickness is adjacent, as in structures (1) and (2), to the sp^3 layer an order of magnitude thicker than the composite layer (see Section 7).

The possibility of multiplexing these structures is discussed. With electric contacts applied and heating these structures on one end and (or) cooling them on the other end, they can be used to manufacture TEGs with record parameters. Estimates show that the combined action of these two effects should result in a 1000-fold increase in the ZT parameter under ideal conditions. Even if the use of carbon nanostructures in TEGs does not ensure the achievement of record parameters, which are an order of magnitude better than those of the existing thermoelements, an improvement in parameters by a few tens of percent would be already very important for developing a new area of studies of thermoelements based on nanostructures.

2. Thermal emf in carbon nanostructures. Mechanism of ballistic phonon drag of electrons

2.1 Qualitative picture of ballistic phonon drag of electrons

Phenomena of interest to us are based on the interaction of electrons with crystal-lattice vibrations in a nanostructure. Consider the qualitative picture of this interaction (Figs 3 and 4).

Let us assume that a region with the sp^2 hybridization of carbon atoms has the higher temperature T_h than the environment. This means that crystal-lattice vibrations (phonons) in the higher-temperature region are excited more strongly than in the region at the lower temperature T_c. Consider the collision of phonons coming from the heated region with an electron absorbing phonons moving in the electron gas in the sp^2 region. Electron drag involves electron propagation in space in the direction of the momentum of the phonon absorbed by the electron. Clearly, in a uniformly heated sample, no directional phonon drag of electrons appears, and the electron gas distribution does not change. If a temperature gradient exists, it creates such a predominant direction. Electrons are displaced. The electron concentration in the cold region somewhat increases compared to that in the heated region. A potential difference appears and an electric field $\mathbf{E}$ is produced, directed opposite to the temperature gradient. This phenomenon is namely the thermoelectric effect $\mathbf{E} = -\gamma\nabla T$.

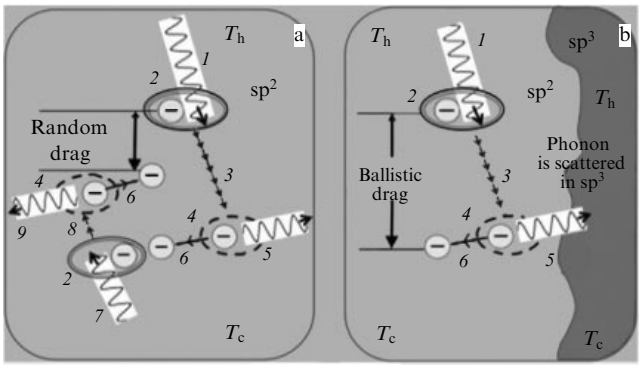

Figure 3. Drag of electrons by phonons (phonon wind). Hot regions T_h, cold regions T_c. Wavy lines (*1*, *5*, *7*, *9*) show the motion of phonons; thick lines (*2*) distinguish regions where a phonon is absorbed by an electron; lines of short arrows (*3*, *8*) show a combined motion, the phonon drag of electrons; dashed lines distinguish regions (*4*) where decay occurs in which a phonon is detached from an electron; lines of long arrows (*6*) show the motion of electrons after the end of the drag process. (a) Drag by chaotic phonons in the region with sp^2 hybridization only. Drag (*3*) of electrons by phonons (*1*) moving from 'hot' to 'cold' is partly compensated by the drag (*8*) by phonons moving from 'cold' to 'hot' (*7*). Both a phonon (*9*) and an electron remain in the sp^2 region. The result is random drag. (b) Ballistic phonon drag. After the drag (*3*) of electrons by phonons (*1*) moving from 'hot' to 'cold' and decay (*4*), the electron remains in the sp^2 region, while phonon (*5*) is absorbed by a 'cooler' — the sp^3 region. The result is ballistic drag.

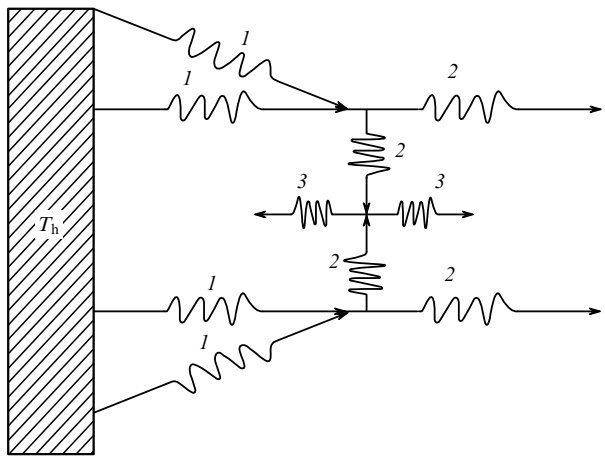

Figure 4. Randomization of phonons *1* emerging from the 'hot' region T_h. These phonons move from 'hot' to 'cold'. After a collision, phonons *2* appear. After the collision of phonons *2*, phonons *3* appear. Among phonons *3*, phonons moving from 'cold' to 'hot' exist.

Figure 3a shows the situation in an sp^2 sample no more than ten nanometers in size. Along with the drag of electrons by phonons coming from the heated part of the sample and having the momentum directed opposite to the temperature gradient, there is a drag of electrons by phonons coming from the cold part with the momentum directed along the temperature gradient. The drag by phonons from the cold region partly compensates the drag by phonons coming from the heated region of the carbon nanostructure (Fig. 3a).

Phonons move randomly in all directions. 'Cold' phonons are created, in particular, in collisions between phonons emitted during the combined motion of electrons with phonons absorbed by them if after the decay (emission) the emitted phonons remain in the same sample with the sp^2 hybridized carbon atoms. The 'randomization' of phonons can also occur for another reason in an sp^2 sample not of nanometer size. Phonons emitted from the heated region, but not absorbed by electrons, can pass to random motion (see Fig. 4).

In the case of random phonon motion, the thermal emf coefficient produced by the phonon drag of electrons is inversely proportional to the temperature [2]. The smaller the contribution of the random component to the phonon energy, the more efficient the effective displacement in the temperature gradient direction and, therefore, the higher the thermal emf coefficient.

Namely such a phonon drag effect involving randomly moving phonons was considered by my teacher Lev Emmanuilovich Gurevich. He performed this study between 1940 and 1946. In 1940, he published the world's first monograph on physical kinetics [128] containing the chapter "Electronic processes in solids" and sections "Electronic

process in metals" (§ 19) and "Kinetic equation for electrons in metals" (§ 20). These sections are based on the book *Theory of Metals* by Bethe and Sommerfeld [129]. In these books, no 'drag' is present yet. In 1946, Gurevich published an article "Thermoelectric properties of semiconductors" [2] in the *Journal of Experimental and Theoretical Physics*. The abstract of the article reports: "The article studies a new, so far not investigated mechanism of formation of a thermoelectric force (thermal emf) due to the drag of electrons by a phonon flow produced by a temperature gradient...." Gurevich later returned to this problem many times. Some his pupils developed under his leadership the theory of phonon drag of electrons. However, I did not perform such studies with him.

Another situation (Fig. 3b) takes place in a carbon nanostructure, which is unique because the sp^2/sp^3 sample consists of regions with contrasting physical properties separated by a very small distance, less than one nanometer. Electrons are dragged by phonons coming from the heated region, but after the end of their combined motion (after the decay of an electron–phonon pair), the appearing phonons do not collide with each other and their randomization does not occur. Such emitted phonons pass, at least partially, from the sp^2 to the sp^3 region and remain there, being absorbed! The same occurs with some of the phonons appearing during the randomization of phonons emitted from the heated region, but not absorbed by electrons. In the first qualitative approximation, we can assume that the number of phonons producing the displacement along the temperature gradient is small — they are simply absent! Nothing prevents the drag by phonons from the hot region, the reverse displacement being absent! Phonons emitted from the heated region can be reasonably called 'ballistic' because they fly like stones from a ballista.

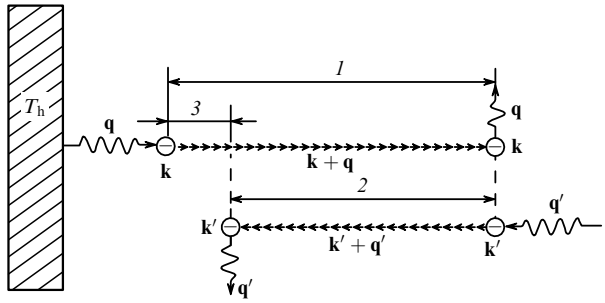

Figure 5. Diagram of the drag process shown in Fig. 3. Wavy lines show the motion of phonons; the lines of short arrows show the combined motion — the phonon drag of electrons. Distance *1* corresponds to the drag of electrons by ballistic phonons moving against the temperature gradient. Distance *2* corresponds to the drag of electrons by phonons moving along the temperature gradient. Distance *3*, the difference between displacements *1* and *2*, is the result of the random phonon drag of electrons. The displacements of electrons after the drag and decay are disregarded. Other explanations are presented in the text.

2.2 Quantitative theory of ballistic phonon drag of electrons

2.2.1 Formulation of the problem of ballistic phonon drag of electrons in carbon nanostructures. Consider the interaction scheme (Fig. 5) producing the thermoelectric effect due to the phonon drag of electrons. Assume that a sample contains a region at a higher temperature T_h than the environment. A phonon with the wave vector $\mathbf{q}$ and energy $\hbar\omega_{ph}$ is a particle corresponding to crystal-lattice vibrations at frequency ω_{ph} in this region. We will find the probability of a collision of this phonon with an electron with the wave vector $\mathbf{k}$ and energy close to the Fermi energy ε_F which will absorb with some probability this phonon moving in the electron gas in the region with sp^2 hybridized carbon atoms. Let us assume that the very first collision of the phonon occurs with an electron. This scenario is typical for small samples.

The absorbed phonon imparts to the electron not only its energy but also momentum. The phonon drag of the electron leads to the additional displacement of the electron in the direction of the momentum of the absorbed phonon. These displacements are indicated in Fig. 5 by arrows *1* and *2*. The phonon drag of an electron is an elastic process. For example, at the end of displacement *1*, decay occurs, and a phonon is emitted with the same wave vector $\mathbf{q}$, but moving in an arbitrary direction. Of course, the electron is also displaced during the decay, but this displacement is small.

A unique property of the carbon nanostructure is the way *1* lies in the graphite-like sp^2 hybridized region of carbon atoms, but a phonon appearing at the end of this segment can enter the diamond-like sp^3 hybridization region. Because of the high heat capacity of the diamond-like region, phonons remain in it. Thus, in this case, the phonon leaves the sp^2 region, in which the drag occurs, while electrons remain in it after the drag. Electrons do not enter the dielectric diamond-like region. This is the qualitative picture of the ballistic phonon drag of electrons considered in Section 2.1 and presented in Fig. 3b.

In sp^2 regions ten nanometers in size, a noticeable probability (see Section 2.2.2) exists that the very first collision of a phonon emitted from a region at temperature T_h will occur with an electron, and this electron will absorb the phonon and will be displaced along the phonon motion direction, i.e., will be dragged (see Fig. 5). The electron wave vector and energy in the final state are written as $\mathbf{k}+\mathbf{q}$, $\varepsilon_k + \hbar\omega_q$, respectively, while the number of phonons will be $N_q - 1$. This process is naturally interpreted as the absorption of a phonon by an electron. An elastic decay process of phonon emission by an electron also exists. The wave vectors $\mathbf{k}$ and $\mathbf{q}$ and energies ε_k and $\hbar\omega_q$ will return to their previous values, but the number of phonons in the final state increases to $N_q + 1$. This is phonon emission, and the electron comes into equilibrium again.

When phonons move randomly (Fig. 3a), the picture is different. In this case, electrons are displaced not only opposite but also along the temperature gradient. Such a process is shown schematically in Fig. 5 by arrow *2*. The wave vectors of the phonon and electron involved in this process are primed. Clearly, the resulting displacement of the electron against temperature gradient (*3*) in this case is much smaller than displacement (*1*) during the ballistic drag.

These processes are of a higher order than individual phonon–phonon or electron–electron interaction. The drag process corresponds to the consideration of anharmonic terms in vibrational energy.

Phonon–phonon collisions can be ignored because of the smallness of the region; however, elastic electron–phonon collisions should be taken into account. The qualitative picture of the ballistic phonon drag of electrons (see Section 2.1 and Fig. 3) shows that the electron concentration changes due to the phonon drag of electrons. This produces the thermoelectric effect.

It follows from dimensionality considerations that the thermal emf coefficient can be written in the form $\gamma = \alpha k_B/e$, where k_B is the Boltzmann constant, e is the electron charge,

and the dimensionless thermal emf coefficient α reflects all the numerous mechanisms producing the thermoelectric effect. The coefficient α is often called, like γ, the thermal emf coefficient, adding 'dimensionless' sometimes.

In metals and graphite, which is a semimetal, the electron concentration and, in fact, electron energy are independent of temperature, and therefore the thermal emf of metals caused by diffusion is small compared to the thermal emf of semiconductors (see, e.g., [130, Ch. 11]).

However, it is not quite so. Experiments show that the thermal emf coefficient in semimetals is not small. The value of α is not of the order of 0.01, as follows from the theory, but is about 0.1 or even unity. A F Ioffe was the first to point out back in 1929 the prospects of using semimetals for creating thermoelectric generators. The thermal emf of metals is in the best case ten μV K^{-1}. The thermal emf coefficient of impurity semiconductors and metals is about a few hundred μV K^{-1}. Even before the Great Patriotic War, Ioffe and his coworkers at the Physical-Technical Institute, Leningrad, managed to create thermoelements with an efficiency ZT of about 0.03 [130].

Thus, the thermal emf coefficient of metals related to the mechanisms of diffusion and the drag of electrons by randomly moving phonons can be written as (see [131], § 68)

$$\gamma = \frac{k_B}{e}\left(A\,\frac{k_B T}{\varepsilon_F} + B\,\frac{\theta}{T}\right). \qquad (1)$$

Coefficients A and B are of the order of unity. The first term in (1) is determined by diffusion and the second term, by the drag of electrons by randomly moving phonons.

In semimetals, the second term is much greater than the first. To compare terms in (1), note that the Debye temperature θ and the Fermi energy ε_F in the same crystal are related to each other. The parameters of the electronic spectrum of a metal are expressed in terms of the lattice constant a and the effective electron mass m. Thus, the Fermi momentum is $p_F \sim \hbar/d$ ($a \sim d$, d is the size of the sp^2 region), the Fermi velocity is $v_F = p_F/m \sim \hbar/(ma)$, and the Fermi energy is $\varepsilon_F \sim v_F p_F \sim \hbar^2/(ma^2)$. The parameters of the phonon spectrum can also contain the atom mass M. The matter density ρ is proportional to the mass M, $\rho \sim M/d^3$, and the sound velocity (phonon velocity) can be written as $c_s \sim (p/\rho)^{1/2}$, where p is pressure. This means that the phonon velocity is proportional to $M^{-1/2}$. It follows from dimensionality considerations that c_s is proportional to $(m/M)^{1/2}$, and therefore $c_s \sim v_F(m/M)^{1/2}$. We ascertain that the Debye temperature is related to the Fermi energy as

$$k_B\theta \sim \hbar\omega \sim \frac{\hbar c_s}{d} \sim p_F c_s \sim p_F v_F\left(\frac{m}{M}\right)^{1/2} \sim \varepsilon_F\left(\frac{m}{M}\right)^{1/2}.$$

By substituting this estimate of ε_F into the expression for the thermal emf, we see that the second term in (1) dominates in the entire temperature range because $B \gg A(m/M)^{1/2}$ and $\theta/T \gg T/\theta$. Recall that the Debye temperatures for graphite along graphene planes and in the perpendicular direction are 760 and 2280 K, respectively.

Thus, the thermal emf in semimetals, in particular, in graphite, is determined by the phonon drag of electrons rather than by diffusion.

We can conclude that the thermal emf produced by diffusion calculated for a metal $\gamma \approx (k_B/e)(k_B T/\varepsilon_F)$ is anomalously small because of the factor $\alpha \approx k_B T/\varepsilon_F$. All this means that, in the region with sp^2 hybridized carbon atoms, it is necessary to take into account elastic phonon–electron interactions resulting in the directly proportional temperature dependence of the thermal emf coefficient γ: the first term in expression (1) for γ is small, and second-order terms produced by anharmonic vibrations can exceed it. This contribution is produced by the ballistic phonon drag of electrons. Let us analyze this process. A qualitative consideration is not sufficient here, because the probability of this process is unknown.

2.2.2 Estimates of characteristics of carbon nanostructures. We determine first the conditions of the propagation of phonons in a graphite-like region. Let us estimate the mean free path l of phonons in a carbon nanostructure [131, 132]. A rough estimate can be made from the classical relation for vibrations of a carbon atom with mass $M \approx 12$ a.m.u. with the characteristic deviation ξ, namely, from the energy relation $M\omega^2\xi^2 \approx k_B T$. The characteristic frequency is $\omega \approx c_s/a$, where $c_s \approx (2-5)\times 10^3$ m s^{-1} is the sound velocity in sp^2–sp^3 hybridized carbon. Here, c_s is assumed to be the velocity of long-wavelength acoustic phonons, which make the main contribution to the drag effect [2]. Then, the mean free path is [131, 132]

$$l = \frac{M c_s^2 a}{k_B T} \approx 5\ \text{nm}.$$

This value gives an estimate of the sp^2 hybridization region $d \approx 2-4$ nm in which phonons propagate without mutual collisions, i.e., ballistically [132]. In a region of this size or smaller, phonons propagate without randomization ($l > d$). The ballistic propagation regime allows us to calculate the phonon flux intensity r as that of the radiation flux at wavelength λ from a blackbody for phonons. We have

$$r = \frac{4\pi^2\hbar c_s^2}{\lambda^5}\left[\exp\left(\frac{2\pi\hbar c_s}{\lambda k_B T}\right) - 1\right]^{-1}. \qquad (2)$$

We will now determine conditions in which electrons are found. In the sp^2 region, electrons represent a degenerate gas. The degeneracy temperature

$$\frac{\hbar^2}{k_B m a^2} \approx 10^5\ \text{K} > T$$

is much higher than temperatures at which TEGs operate. It was shown in [1] that quantum-size effects can be ignored if the size of the regions in carbon nanostructures exceeds 3 nm (see [133, §§ 22, 23]. Below, we consider only samples in which quantum-size effects are absent in the sp^2 region for both phonons and electrons.

Note finally in the formulation of the problem that electron–phonon interaction at temperatures above 10 K involves namely the absorption of longitudinal acoustic phonons [134, 135].

2.2.3 Probability of ballistic phonon absorption by an electron. Let us now estimate the probability of interaction of an electron from a degenerate electron gas with phonons (see Fig. 3, points *2*). When phonons move randomly and the Debye temperature is $\theta < T$, from the displacement of an electron absorbing a phonon and moving from 'hot to cool',

the displacement of the same electron (see Fig. 5) by a phonon moving from 'cold to hot' is in fact subtracted. As a result, the thermal emf coefficient proves to be proportional to θ/T.

For ballistic phonons, the situation is completely different. All the absorbed phonons propagate against the temperature gradient, while phonons emitted by electrons are isotropic, and we can assume that the emission of phonons has no effect on average on the drag of electrons by a flow of ballistic phonons.

Thus, the calculation of drag characteristics in this case is considerably simplified. It is sufficient to find the probability of phonon absorption by an electron, whereas the probability of electron displacement along the momentum of the absorbed phonon is 100%.

The scattering probability per unit time is calculated from the known quantum-mechanical expression, which, in the form that is the most convenient for the formulated problem, is presented in [135, Ch.VIII, § 3]. Details of calculations can be found in [1]. As a result, we obtain the rate of absorption of ballistic phonons by electrons:

$$W = \frac{4\pi a^3}{d^3}\left(\frac{\hbar^2}{2ma^2}\right)^2 \frac{1}{Mc_s^2}\frac{2\pi c_s}{\hbar}\left(\frac{k_B T}{2\pi\hbar c_s}\right)^3 \Gamma(3)\zeta(3)\frac{d}{c_s}\, d^2 . \tag{3}$$

Here, $\Gamma(3) = 2$ is a gamma function, and $\zeta(3) \approx 1.2$ is the Riemann zeta function. Calculations show that $W > 10^{12}\ \mathrm{s}^{-1}$. Direct experiments [136] confirm, in our opinion, this result.

The electron–phonon interaction probability — the probability of phonon absorption by an electron for the phonon-propagation time d/c_s through a region of size d — proves to be more than 40%. The effect exists!

2.2.4 Parameters of the ballistic drag process in nanosize carbon films. Note first that it is the interaction (absorption) rate W (see (3)) and the motion time $\tau_b = W^{-1}$ of ballistic phonons that have a physical meaning. The probability value determines the size x at which phonons move ballistically until their scattering by electrons and by each other. The value of x is determined by the condition

$$W\frac{x}{c_s} < 1 .$$

If $x > d$, in the entire sp^2 region, the time of motion determining the drag and the corresponding thermal emf coefficient will be $\tau = \tau_b$. If $x < d$, the sp^2 region should be divided into two parts. In one of them, with size x, phonons can be assumed ballistic, whereas in the other part, with size $d - x$, phonons move chaotically. In the region of ballistic propagation of phonons through a degenerate electron gas, only the displacement of phonons against a temperature gradient takes place.

Let us formulate qualitative results. First, the time of motion of phonons in the ballistic regime $\tau_b = W^{-1}$ is inversely proportional to the third power of the temperature of the heated region of the graphite-like region. Second, the probability of absorption of a ballistic phonon by an electron and, therefore, the drag probability is proportional to the size x of the region of propagation of ballistic phonons.

Obviously, a new process of absorption of ballistic phonons by electrons considered here gave a new temperature dependence of the thermal emf coefficient. The thermal emf coefficient γ_b corresponding to the drag of ballistic phonons can be estimated by replacing the Debye temperature θ in the expression (see (1))

$$\gamma = \frac{k_B}{e}\, B\, \frac{\theta}{T}$$

for random phonon drag by some new 'effective' temperature $\hbar W/k_B$ of ballistic phonons. We obtain

$$\gamma_b = \frac{k_B}{e}\, B_b \frac{\hbar W}{k_B T} . \tag{4}$$

Obviously, the contribution to the thermal emf coefficient produced by the ballistic phonon drag is an order of magnitude greater than that for random phonons in the same material and reaches $10^3 - 10^4\ \mu\mathrm{V\ K}^{-1}$.

As pointed out above, electron displacements l caused by ballistic phonon drag greatly exceed those in the case of random phonons. These displacements are approximately equal or smaller than the graphite lattice constant $a = 0.35$ nm. On the other hand, the drag is possible only at distances comparable to the phonon mean free path. The thickness of sp^2 layers that can be achieved using modern technology (see Section 3) is not smaller than $l = 50$ nm. By simplifying expression (4) and replacing the dimensional thermal emf coefficient $\gamma = \alpha k_B/e$ by the dimensionless thermal emf coefficient α (see also [1]), we obtain

$$\alpha_b \approx \left(\frac{2\pi k_B T l}{h c_s}\right)^2 . \tag{5}$$

The numerical factor is set equal to unity ($c_s \approx 1.5 \times 10^3\ \mathrm{m\,s}^{-1}$ is the speed of sound in the sp^2 region). Estimates show that the thermal emf coefficient ($\alpha \approx \alpha_b$) is equal as a minimum to 600–700 at temperatures $T \approx 3 \times 10^2$ K. This means that the thermal emf coefficient is $\gamma \approx 50\ \mathrm{mV\ K}^{-1}$. We will assume that the electric conduction of an sp^2 film coincides with the tabulated value $\sigma \approx 2500\ \mathrm{S\ m}^{-1}$ presented in handbooks for carbon electrodes, while the heat conduction of thin sp^2 layers considerably exceeds the tabulated heat conduction of graphite and is equal to $\chi \approx 2000\ \mathrm{W\ m}^{-1}\ \mathrm{K}^{-1}$ [137]. Thus, the efficiency of a thermoelectric generator $ZT = T\gamma^2\sigma/\chi$ can reach $ZT \approx 20$ at room temperature. Recall that the efficiency of the best of the existing TEGs [1, 138] is $ZT \approx 1.5$ at room temperature.

Obviously, the effective temperature $\hbar W/k_B$ should not be used in the 'diffusion' term of the thermal emf coefficient (1). The diffusion term appears due to electron–electron rather than electron–phonon interaction. In the case of the random phonon drag of electrons, the thermal emf coefficient is inversely proportional to temperature [2]. Note that the thermal emf coefficient in the case of the ballistic phonon drag of electrons is proportional to the temperature squared.

3. Thermoelectric generator based on film carbon nanostructures

The technology for preparing films made of graphite-like materials for the development of thermoelectric generators was experimentally demonstrated in [126] (Fig. 6). The technology can provide the homogeneity and small enough thickness of such a film and can ensure its location on a diamond-like film with prepared contacts (Fig. 7) with the acceptable interface (Fig. 8).

Figures 6–8 show a structure consisting of two types of films with sp^2 and sp^3 hybridized carbon atoms, i.e., this

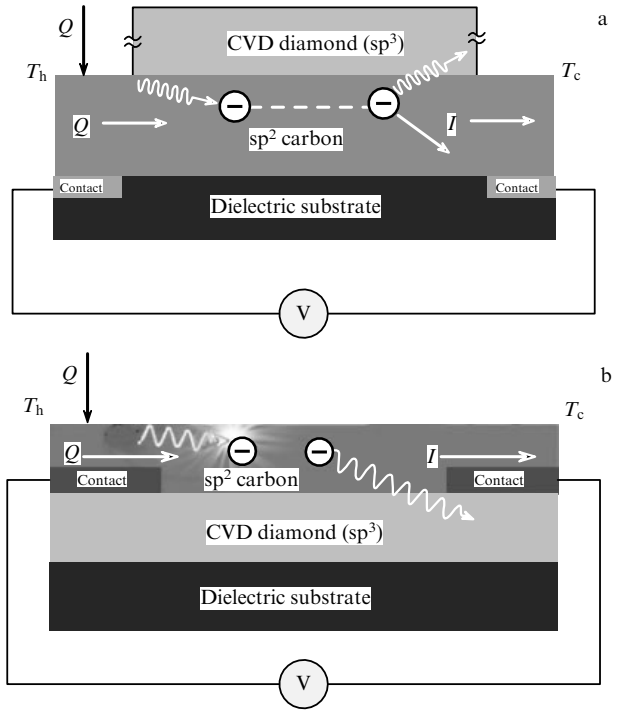

Figure 6. TEG prototype with the film structure prepared by the CVD method. The drag process is shown as in Fig. 3b. The heat Q in a heated region with temperature T_h is transformed into the electron flow I flowing in the sp^2 region from a contact in the hot region to a contact in the cold region with temperature T_c. (a) The sp^2 layer on a substrate is covered with the sp^3 layer. (b) The sp^3 layer on a substrate is covered with the sp^2 layer. Each of these procedures has its technological advantages and disadvantages [108, 109].

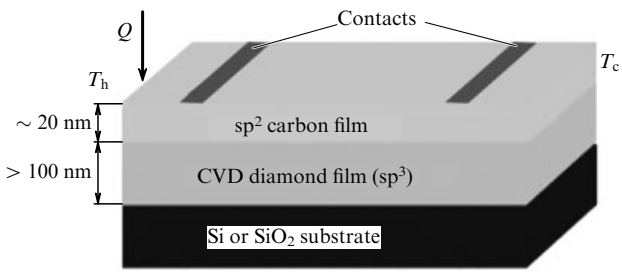

Figure 7. Optimal TEG with the sp^2/sp^3 film structure.

structure consists of graphite-like and diamond-like regions. The diamond-like film is a peculiar 'cooler' removing heat from the graphite-like film. The diamond-like film can be located either under (Figs 6b, 7) or above (Fig. 6a) the graphite-like film. During the growth of the films, an interface appears between them (see Fig. 8). Theoretically, the interface thickness should be smaller than 1 nm. This is a unique feature of carbon nanostructures (see Section 1). Different methods for the deposition of films on each other [125, 126] cannot provide an interface thickness smaller than 10 nm. Measuring the interface thickness is very complicated and therefor unreliable, as pointed out in [125, 126].

Between the sp^2 and sp^3 films, a temperature difference and phonon flow appear. The phonon flow drags the electron gas in the sp^2 film and produces a thermoelectric field.

Calculations of the drag efficiency and thermal emf coefficient determined by the drag effect (see Section 2)

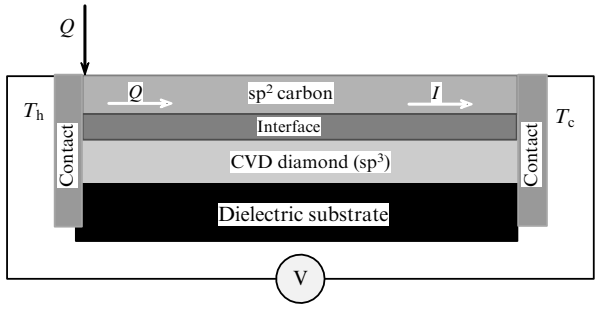

Figure 8. TEG prototype with which the thermal emf coefficient in a film structure was measured. An sp^3 layer on a substrate is covered with an sp^2 layer. The measurement of the important interface thickness is complicated.

showed that the thermal emf coefficient exceeds by orders of magnitude the known values for graphite, $\approx 10-20$ μV K^{-1}, in the temperature range slightly above room temperature.

Measurements show that the drag effect provides thermal emf values that are two orders of magnitude greater than in the case of the diffusion process. The placement of a graphite-like (sp^2) material on a diamond-like (sp^3) film provides the increase in the thermal emf. This is caused by the ballistic phonon drag of electrons. Thus, conditions required for the development of TEGs based on carbon nanostructures can be achieved.

At present, applications of carbon films with sp^2 hybridized carbon atoms for the development of TEGs are extensively being studied [1, 126]. The devices used in experiments are protected by a patent [110]. Various aspects of the phonon drag of electrons such as the Gurevich effect and ballistic phonon drag in carbon films are studied in experiments. The contribution of this effect in macroscopic samples does not exceed typical values for the diffusion contribution and is about 50 μV K^{-1} in the best existing TEGs. Detailed investigations were recently performed again in the hope of developing graphene-based TEGs [138, 139] (see Section 7).

The theory predicts that the ballistic phonon drag of electrons can provide the value of $\gamma \approx 1.50$ mV K^{-1} [110] (see Section 2). Based on these calculations, the design of a TEG with record parameters was proposed in [140]. It is being proved at present [126] that such TEGs can be developed based on carbon film nanostructures that can be produced using modern technology.

Films consisting of layers of a graphite-like sp^2 material with a highly-ordered crystal lattice are prepared by different methods at synthesis and annealing temperatures of about 1000 °C or higher. These temperatures exceed the typical temperature of growing diamond films on different substrates by the CVD method, which can change the phase composition and damage the mechanical properties of the sp^3 layer due to thermal action during the deposition of the sp^2 layer on it. To achieve the technological compatibility of the deposition processes of sp^3 and sp^2 hybridized carbon atoms, technological setups for producing graphite-like sp^2 films at temperatures not exceeding those used in the CVD method for growing sp^3 layers were investigated.

Graphite-like films were prepared by the microwave plasma chemical vapor deposition (MWPCVD) of a graphite target in the direct current regime.

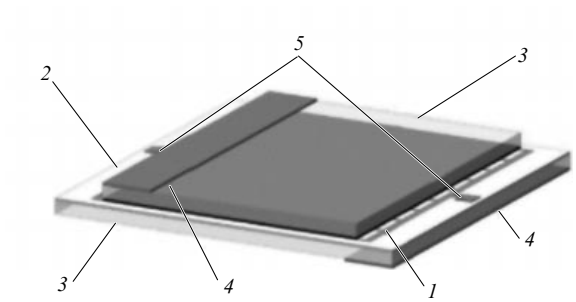

Figure 9. Diagram of a TEG used to measure the thermal emf coefficient in a film structure. Two-layer system used in experiments: *1* — thin graphite-like sp^2 film prepared by magnetron deposition; *2* — sp^3 polycrystalline CVD diamond; *3* — silica substrate and pressing plates at the bottom and top; *4* — heating region located at the top left on the sp^2 layer, cooling region at the bottom right under the sp^2 layer; *5* — electric contacts located between sp^2 and sp^3 layers. Other details in the text.

The thickness of films made of the sp^2 material was measured in the range of 20–140 nm by the methods of scanning electron microscopy (SEM), probe profilometry, and scanning probe microscopy (SPM). The results coincided. The SEM method could not provide reliable film thickness measurements below 20 nm.

In experiments [126], the sp^3 layers were for the first time grown on layers with a high content of sp^2 carbon. No other reports about such experiments were found in the literature. Studies of technological instruments for the preparation of alternating graphite-like and diamond-like films have demonstrated the possibility of creating structures with three or more alternating layers used in a thermoelectric generator.

The TEG design used in experiments [126] is shown in Fig. 9. Thermoelectric characteristics were measured with the simplest two-layer system. First, an sp^3 diamond-like layer was grown on a 16×16-mm quartz substrate, then a system of gold contacts was deposited by photolithography. This was followed by the deposition of a working layer (a graphite-like film with heated and cooled regions on the edges) on gold contacts. To build a measurement setup, it was necessary to boil soft and package the obtained two-layer sample. Then, a quartz plate cover was fixed on the surface of the packaged substrate with the sp^3/sp^2 layers and the rod contact leads of the boiled substrate. The whole system was fastened with clamping plates.

A sample was heated to $250-300\,^{\circ}C$ on one of the sides of the plate with a contact heater. The heater temperature was measured with a thermocouple. Cooling was provided with a water-immersed copper rod pressed against the sample. The temperature of the cooled part was measured with a pyrometer. Typical thermal emf values measured for a ~ 100 nm sp^2 film deposited on the surface of a diamond-like film were one–two orders of magnitude greater than the typical value of 3×10^{-5} mV K^{-1} for macroscopic pyrolytic graphite. Obviously, the diamond-like sublayer provides an increase in the thermal emf of the element. The values obtained strongly depend on the location of the contacts; however, the effect was always observed. The main difficulty in the preparation of experiments was the necessity of obtaining a sharp enough transition layer (interface) about 10 nm in width between carbon films with the sp^2 and sp^3 hybridized electron shells.

The technological instruments for depositing alternating sp^3 layers, the basic material (BM) of the thermoelement, and sp^2 layers, the additional material (AM) of the thermoelement, were experimentally studied separately [125]. These investigations involved the successive deposition of the sp^3 layer by the MWPCVD method at low methane concentrations in the working mixture ($< 1\%$). Next, a layer of the sp^2 material was deposited by the same MWPCVD method at high methane concentrations ($> 10\%$). Then, an sp^3 layer was again deposited at low methane concentrations in the working mixture ($< 1\%$).

Structural studies of three-layer materials consisting of alternating BM and AM films were performed by the SEM method, giving images of cross sections of the structures at different stages of their creation. The thickness of the sp^3 and sp^2 films in multilayer structures was 160–310 nm and 40–150 nm, respectively. It is unlikely that theoretical predictions can be completely realized at such thicknesses of the sp^2 films; however, experimental data obtained demonstrate without a doubt the contribution of the thermal emf mechanism based on the ballistic phonon drag of electrons.

A TEG based on multilayer carbon nanostructures of alternating sp^2 and sp^3 films was patented [109]. The problem was the development of a thermoelectric element with the simpler construction preserving the high thermal emf coefficient.

This problem was solved using a thermoelectric element consisting of a carbon BM with the sp^3 hybridization of atomic bonds and a carbon AM with the sp^2 hybridization. A new feature is that the BM consists of at least two films with an AM film located between them. In this case, the BM film thickness (d) and the AM film thickness (b) should satisfy relations $2 \leqslant d \leqslant 50$ nm and $1 \leqslant b/d \leqslant 100$, and electric contacts should be deposited on the opposite peripheral AM regions.

Figure 10 shows the vertical section of a TEG consisting of many separate elements similar to Figs 6–8. As pointed out in [109], a multilayer TEG is also made by the CVD method.

A TEG battery is built by forming first one element. Then, the next AM layer is deposited on a BM layer covering an AM and contacts in the element already prepared. The contacts are then deposited on the AM layer, and a BM layer is grown on these contacts. This process is repeated the number of times needed to build the required thermoelectric battery.

The TEG begins to operate when a temperature difference is produced between the contacts. If one contact and (or) an AM region adjacent to it is cooled, whereas the other contact and (or) an AM region adjacent to it is heated, an electric current will flow in the external circuit between contacts.

At present, experiments with a TEG of this design continue.

We can conclude that the idea of using the ballistic phonon drag of electrons to increase the thermal emf coefficient γ proves to be realizable in practice! The location of a graphite-like material on a diamond-like film ensures an increase in the thermal emf due to the ballistic phonon drag of electrons.

We can say that the technological level will ensure the development of carbon nanostructures for creating TEGs with record parameters. The unique location of these materials very close to each other inherent only in carbon nanostructures guarantees the removal of phonons emitted by electrons from sp^2 regions after their combined motion, which allows us to expect the achievement of a thermal emf up to 0.1 mV K^{-1}.

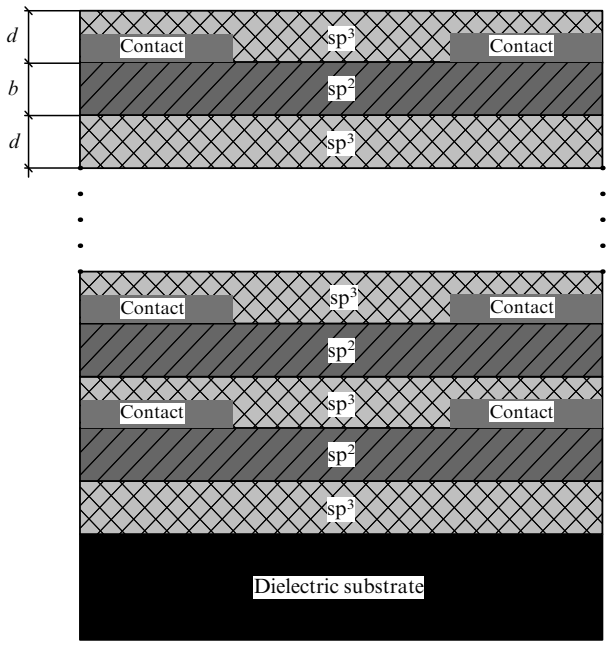

Figure 10. Proposed TEG includes: a substrate made of materials selected according to the requirements of the manufacturing technology; the main material sp^3; the additional material sp^2; contacts selected according to the technology requirements. The vertical section of an individual element is shown at the top. The repetition of an individual element is shown by three dots. One of the contacts is hot and the other cold. Other explanations in the text.

4. Thermal conduction in carbon nanostructures. Mechanism of heat transfer through the sp^2/sp^3 hybridization region interface of carbon atoms

4.1 Qualitative picture of heat transfer through the sp^2/sp^3 region interface

At present, there are a few models for explaining phenomena observed during heat transition through the sp^2/sp^3 region interface.

The first model, proposed by I M Khalatnikov more than 60 years ago [141], analyzes the phonon heat transfer through the interface. The phonon flow is considered in the approximation of an elastic continuous medium, and the influence of phonons on electrons in a metal is ignored. For phenomena on the dielectric–metal interface, this model predicts even at low temperatures a temperature jump two orders of magnitude smaller than observed in experiments [142–145]. The updated model proposed in paper [146] assumes that the energy transfer occurs when phonons coming from a dielectric to a metal interact with electrons in the metal. Phonons are considered in the same approximation as in Khalatnikov's model, while electrons are treated as gas. Both these models are valid only at low temperatures, because only low-frequency (LF) vibrations correspond well to processes in a continuous medium. At high temperatures, high-frequency (HF) crystal-lattice vibrations are also excited, which do not correspond to such models.

The model proposed in [147] assumes that phonons in a metal and a dielectric exist independently. In our opinion, this model is valid only at very high temperatures when vibrational frequencies of a crystal lattice in a dielectric are high. Transitions of phonons from a dielectric to a metal at high temperatures can be disregarded.

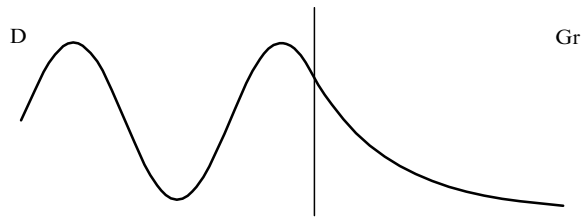

Figure 11. Propagation of vibrations along two different coupled semi-infinite one-dimensional chains for the vibration frequency in a dielectric (diamond-like region D) exceeding the maximum possible vibrational frequency in a metal (graphite-like region Gr). The straight line shows the boundary of regions. High-frequency vibrations penetrate into the metal but decay in it.

This is demonstrated in paper [148], where the last of the known models of heat transfer through an interface is presented. However, in [148], only the case of the interface between two dielectrics is considered. In [149, 150], the idea proposed in [148] was applied to the dielectric–metal interface at room temperature, which is very important for estimates of TEG efficiency. Of course, this theory can also be applied to heat propagation through the graphite-like region–metal and diamond-like region–dielectric interfaces, heat propagation in the sp^2/sp^3 region interfaces in carbon nanostructures.

Heat transfer through the sp^2/sp^3 interface in addressing TEG development was studied in [7].

Consider the transition of a wave through the interface when the frequency of the wave incident from a dielectric to a metal exceeds the maximum natural vibrational frequency of the metal, but is, of course, lower than the maximum natural frequency in the dielectric.

Such vibrations are discarded in all the known models. At the same time, it is well known (see, e.g., [151], p. 224) that the Debye temperature in dielectrics greatly exceeds that in metals. This difference is especially great for a composite in which the dielectric is diamond. Our consideration below is applied namely to this composite.

Figure 11 illustrates the solution to the problem of vibrations propagating in a system of two different coupled semi-infinite one-dimensional chains for the vibrational frequency in a dielectric exceeding the maximum possible vibrational frequency in a metal.

The following qualitative picture of the transition of waves through the metal–dielectric interface was obtained: HF vibrations penetrate from a dielectric into a metal, but rapidly decay during their propagation from the sample surface inside the sample. On the one hand, waves do not propagate over the entire metal as do the waves considered in models based on the elastic continuum approximation, and, on the other hand, we cannot assume that these waves do not penetrate into a metal as do the vibrations considered in model [147]. Such waves near the surface also differ from well-known Rayleigh waves [152]. They appear on the side of the interface between two crystals where the speed of sound is greater. In the case of a metal–dielectric interface, Rayleigh waves appear on the dielectric side. On the contrary, the waves considered here appear on the side where the Debye frequency is smaller, i.e., in a metal. Obviously, the penetration of waves from a dielectric into a metal causes HF vibrations of the metal crystal lattice and the energy of these vibrations is transferred to the electron gas. In this way, the energy is transferred from a dielectric to a metal. These

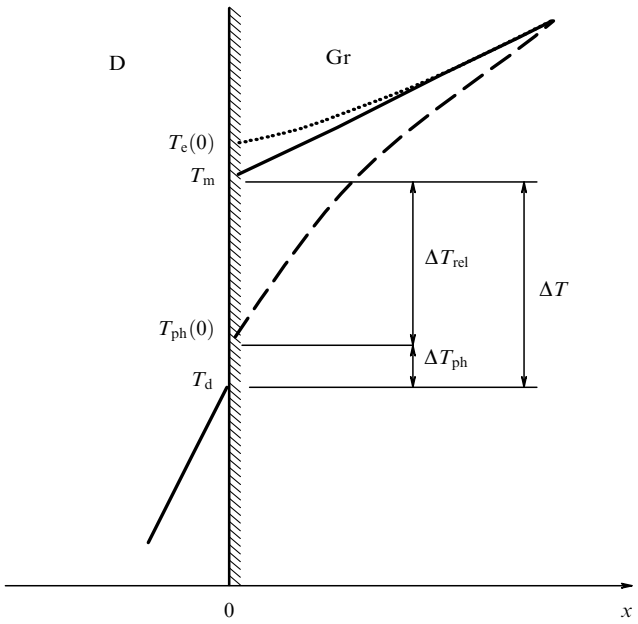

Figure 12. Temperature profile at the dielectric (diamond-like region D)–metal (graphite-like region Gr) interface. The external boundary of the dielectric is cooled. The dielectric temperature at the boundary is T_d. The electron temperature in the metal is shown by the dotted curve; $T_e(0)$ is the electron gas temperature at the interface; the dashed curve is the phonon temperature; $T_{ph}(0)$ is the phonon temperature in the metal at the interface. The solid curve is the extrapolation giving the metal temperature T_m at the interface. ΔT_{ph} is the difference between phonon temperatures at the interface; ΔT_{rel} is the relaxation contribution to the temperature jump. In experiments, the temperature jump ΔT is measured. Other explanations are in the text.

calculations can be generalized to the case of a three-dimensional crystal lattice.

This means that a new model of the energy transfer through the sp^2/sp^3 interface should be realized in carbon nanostructures. This model can explain the thermal properties of diamond–metal composites, in particular, the diamond–graphite composite.

It was shown in [153] that thermal equilibrium in each of the basic subsystems of a metal — the electron gas and lattice — is established faster than equilibrium between the subsystems. It has been assumed so far that this effect should be taken into account only at high currents [153–155]. In this case, the electron gas temperature T_e proves to be higher than the lattice (phonon gas) temperature T_{ph}. Because of the absence of thermal equilibrium, corrections appear to the Ohm and Joule–Lenz laws.

It is easy to assume that the similar overheating or overcooling of electrons compared to the phonon component will also take place at the metal–dielectric interface, in particular, at the graphite-like–diamond-like region interface in a carbon nanostructure composite.

Consider what happens when a metal layer is heated or cooled on one side and is in contact with a dielectric on the other side (Fig. 12). Phonons make transitions from a metal to a dielectric or from a dielectric to a metal, and this thermal flow reduces or increases — due to the Fourier law — the temperature of the metal lattice. The heat from the electron gas does not directly pass to the dielectric. Electrons heat or cool the lattice in a metal and only then does relaxation occur when the heat is transferred to the dielectric through the phonon component. This anharmonic process is the manifestation of the temperature difference between electron and phonon subsystems appearing in the metal due to the presence of the interface with the dielectric.

This situation takes place, for example, when a metal film is deposited on a dielectric substrate or in carbon nanostructures where diamond-like dielectric regions border graphite-like regions with metal properties. The same situation is observed in materials with high-temperature superconductivity and in many other cases. The temperature at the interface of two media always experiences a jump ΔT, which can be assumed proportional in the first approximation to the heat flow q. Such a dependence is similar to Ohm's law, and therefore the proportionality coefficient r between the temperature jump and heat flow $\Delta T = rq$ is called the thermal resistance (or the Kapitza resistance). Obviously, the thermal resistance characterizes the boundary, and its value is very important for any thermal calculations of systems containing medium interfaces.

A similar situation was studied in [156] for the case of a second-order semiconductor. The authors of this paper considered the influence of interfaces between the superconducting and normal phases on the heat conduction of the superconductor.

As shown in [153], the equilibrium in each of the subsystems (electron and phonon) is established faster than between subsystems. This allows each of the subsystems to be described in terms of local temperatures during relaxation. There is an individual contribution to the boundary thermal resistance caused by the establishment of equilibrium during relaxation between the electron and phonon subsystems. This contribution is naturally called the relaxation contribution.

The Kapitza resistance at the metal–dielectric interface was studied in numerous papers. Recent papers are [147, 148, 157]. Each of them proposes a particular model of heat transfer through the interface. However, all these models neglect the anharmonic process in a metal near the interface with a dielectric. At the same time, experiments [158] clearly show the importance of this process in the analysis of heat conduction.

Let us now calculate the Kapitza resistance taking anharmonicity into account.

4.2 Quantitative theory of heat transfer through the sp^2/sp^3 region interface

4.2.1 Formulation of and solution to the problem of heat transfer through the sp^2/sp^3 region interface. Consider a plane metal/dielectric, sp^2/sp^3 interface (see Fig. 12). Each of the materials occupies a semi-space. The coordinate origin is located on the interface. The x-axis is perpendicular to the interface. It is assumed that thermal flows propagate only along the x-axis. In introducing heat conductions of the electron χ_e and phonon χ_{ph} subsystems, it is necessary to use the Fourier equation for each sp^2 subsystem. Recall that Fourier equations relate the thermal and temperature flows of the electron $(q_e; T_e)$ and phonon $(q_{ph}; T_{ph})$ subsystems, respectively.

To solve the problem, it is important to take into account the heat transfer from one sp^2 subsystem to another. This means that

$$q'_e = \theta(T_e - T_{ph}) ,$$

$$q'_{ph} = \theta(T_{ph} - T_e) .$$

The quantity θ characterizes the efficiency of heat transfer between subsystems. The prime means the derivative over x.

At a large distance from the interface, thermal equilibrium exists. The electron and lattice temperatures coincide there, $T_e = T_{ph} = T$, and change identically, providing a constant heat flow $q = -\chi T$ to sp^2 with heat conduction χ. Flows q_e and q_{ph} are components of this total flow. Therefore, $\chi = \chi_e + \chi_{ph}$ and

$$q_e = q\,\frac{\chi_e}{\chi}\,, \quad q_{ph} = q\,\frac{\chi_{ph}}{\chi} \quad \text{for} \quad x \to \infty\,.$$

It is now necessary to set the sp^2/sp^3 boundary conditions, taking into account that the total heat flow to sp^3 is caused only by the propagation of phonons. Therefore,

$$q_e = 0\,, \quad q_{ph} = q \quad \text{for} \quad x = 0\,.$$

One can already see from the formulation of the problem that the properties of a dielectric (in this particular problem, the diamond-like region with the sp^3 hybridization) do not affect the electron and phonon temperatures in a metal (in this particular problem, the graphite-like region with the sp^2 hybridization), and all further results should be the same for the interface between any specified metal and different dielectrics.

The solution to the problem gives the temperatures of subsystems in a metal:

$$T_e = T_m - \frac{1}{\chi}\,qx - \frac{\Lambda q}{\chi}\exp\left(-\frac{x}{\Lambda}\right),$$
$$T_{ph} = T_m - \frac{1}{\chi}\,qx + \frac{\chi_e \Lambda q}{\chi\chi_{ph}}\exp\left(-\frac{x}{\Lambda}\right).$$

The solution contains the characteristic distance from the interface

$$\Lambda = \left(\frac{\chi_e \chi_{ph}}{\theta\chi}\right)^{1/2} \tag{6}$$

on which the electron gas and lattice temperatures are equalized. The solution contains a constant T_m (see Fig. 12) chosen so that the linear extrapolation of T_e and T_{ph} from a region remote from the interface, where these temperatures coincide, would give the temperature T_m at the interface at $x = 0$. It is the temperature jump from T_m to the dielectric temperature T_d that is considered the temperature jump ΔT measured in experiments (see Fig. 12).

The solution also gives the Kapitza resistance r, which should be divided into two parts. The first is the phonon contribution r_{ph} caused by the jump of the lattice temperature $T_{ph}(0)$ (phonons in sp^2) at the interface and of lattice temperature $T_d(0)$ (phonons in sp^3). The second part is the relaxation resistance r_{rel} caused by the temperature jump at the interface due to slow anharmonic heat transfer (relaxation in sp^2) from electrons at temperature $T_e(0)$ to the lattice at temperature $T_{ph}(0)$. It proves to be that [7]

$$r_{rel} = (\chi_{ph}\theta)^{-1/2}\left(\frac{\chi_e}{\chi}\right)^{3/2}.$$

As a rule, $T_e(0) \approx T_m$, and it is assumed that $T_m - T_{ph}(0) = r_{rel}\,q$ (see Fig. 12).

Usually, $\chi_e \gg \chi_{ph}$ in metals. Therefore, the Kapitza resistance caused by relaxation can be expressed in terms of two kinetic parameters characterizing only a metal (sp^2 region). We have

$$r_{rel} = (\chi_{ph}\theta)^{-1/2}. \tag{7}$$

The additional contribution to the boundary thermal resistance described by (7) appears because electrons transferring heat in matter prove to be involved in the heat transfer only near the interface (see Fig. 11). For this reason, the heat transfer through the interface becomes less efficient.

It is assumed in experiments [145, 159, 160] that the temperature linearly depends on the coordinate both inside an sp^3 dielectric (see Fig. 12, region at the left), which is the case, and inside an sp^2 semimetal (the direct line in Fig. 12 at the right), which is incorrect because of the presence of electron gas in it. One can see (see Fig. 12) that the quantity compared to the results of measurements of $\Delta T = T_d - T_m$ can substantially differ from reality. In reality, the phonon temperature difference at the interface is $\Delta T_{ph} = T_m - T_{ph}(0)$. Obviously, this value is smaller than the one that we want to measure. If the electron temperature is measured in a metal at the interface, the temperature jump is $\Delta T_e = T_d - T_e(0)$. This value is greater than the one assumed to be measured in experiments.

The interval of the temperature difference by which temperatures measured and predicted based on the linear extrapolation can differ is

$$\Delta T_{rel} = \Delta T_e - \Delta T_{ph} = \frac{q\Lambda}{\chi}\left(1 + \frac{\chi_e}{\chi_{ph}}\right).$$

This value specifies the relaxation contribution to the temperature jump at the metal/dielectric interface caused by the slow anharmonic heat transfer from the crystal lattice to the electron gas.

4.2.2 Analysis of the heat transfer through the sp^2/sp^3 region interface. Obviously, the temperature and heat conduction jumps should occur during the propagation of the thermal flow through any metal/dielectric interface. However, to verify the existence of the relaxation mechanism of heat transfer between phonon and electron subsystems in a metal, it is convenient to analyze the thermal jump at the interface where the temperature jump (ΔT_{ph}) caused by phonons is small. These results were confirmed by measurements [161–165], but not for the sp^2/sp^3 interfaces.

Therefore, according to the expression representing the thermal analogy of the known Landauer formula [166], the temperature jump does not appear during the propagation of phonons, $\Delta T_{ph} \approx 0$. In this case, the measured temperature difference is ΔT_{rel} and is determined only by the relaxation thermal resistance r_{rel}.

To determine r_{rel} from (7), it is necessary to know the phonon heat conduction χ_{ph} and the efficiency θ of heat transfer between the lattice and electron gas.

The value of χ_{ph} can be estimated from the deviation of the total heat conduction χ of a metal from the Wiedemann–Franz law relating the heat conduction and electric conduction σ. Deviations from this law are caused, first, by the inelastic scattering of electrons and, second, by heat transfer by phonons. In a 'poor' metal, such as a material with sp^2 hybridized carbon atoms, the second reason is more impor-

tant (see [131, p. 528] and [161]). Then, we obtain

$$\chi_{\rm ph} = \chi - \frac{\pi^2}{3e^2}\,\sigma k_{\rm B}^2 T.$$

As already mentioned, the Kapitza resistance calculated from (7) is independent of the characteristics of a dielectric. It is assumed in calculations presented above that electrons are scattered only by phonons, and scattering by defects is ignored.

The efficiency of anharmonic heat transfer between phonon and electron subsystems in a metal can be calculated from the relation in [154], according to which electrons in metals whose heat conduction is mainly determined by the heat conduction of the electron gas are involved in the heat transfer only at a distance of the order of

$$\Lambda = \sqrt{\frac{\chi_{\rm e}}{\theta}}\,.$$

As should be expected, the higher the heat transfer efficiency between subsystems, the smaller the distance at which the temperatures of these subsystems are equalized.

Thus, the relaxation anharmonic interaction between the electron gas and lattice vibrations exists near the sp^2/sp^3 interface. This effect makes an additional contribution to the temperature jump at the interface, which corresponds to the increase in the thermal Kapitza resistance, i.e., the decrease in the heat conduction of the system as a whole. The effect appears because electrons do not transfer heat through the interface and do not receive heat from a dielectric at the interface. As a result, electrons prove to be colder than the crystal lattice.

Thus, except conclusions concerning carbon nanostructures, a general conclusion can be made that the boundary thermal resistance is independent of the dielectric material adjacent to a metal if the phonon propagation coefficient at the interface is close to unity. The boundary thermal resistance depends only on the internal properties of the metal.

The effect discussed above should be taken into account in analyzing phenomena in metal/dielectric structures [2, 167].

4.2.3 Optimal carbon nanostructure composite for a thermoelectric generator. To increase the heat–electric current conversion efficiency, ballistic phonon drag by electrons is used (see Section 2). Thermal losses are reduced using the thermal resistance of interfaces between graphite-like and diamond-like phases of the composite.

Now, it is necessary to predict and confirm experimentally the existence of the optimal structure of the sp^2/sp^3 component. It will be shown below that the structure shown in Fig. 13 is optimal. The economic efficiency of a TEG is mainly determined by the conversion efficiency. The increase in the main efficiency parameter Z of a TEG (showing how many times the heat converted to current exceeds the heat scattered due to the heat conduction), even by a few percent, is already considered an important scientific and practical achievement (see, e.g., [168, 169]).

The author of paper [170], devoted to thermoelectric converters, with the distinctive title "Thermoelectricity, the ugly duckling," published in 2014 in one of the most prestigious scientific journals, emphasizes the long-standing dream of researchers and engineers to turn an 'ugly duckling' into a 'beautiful swan'. However, the ways to fulfill this dream have not been found so far, and the conversion parameter has not been increased even up to three at room temperature.

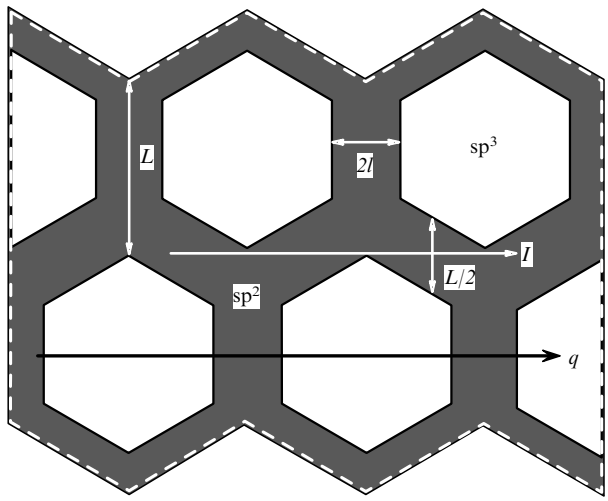

Figure 13. Model of the optimal carbon nanostructure composite. The composite is formed from initial particles in which the sp^3 region remained (white region) and the surface layer became sp^2 (grey region). The edge of the initial particle is L; the distance between the boundaries of sp^3 regions is equal to the doubled thickness l of the sp^2 layer covering each nanoparticle. It is shown that for the optimal conditions for the rectilinear flowing of current, the distance between sp^3 regions in the perpendicular direction should be $L/2$. Electric current I (thin arrow) flows over the sp^2 region and heat flow q (thick arrow), over the entire composite.

A thermoelectric generator based on a matrix sp^2 structure with diamond nanoparticles can open, in our opinion, a possible way to solve this problem.

The high-temperature, high-pressure (HTHP) sintering of carbon nanomaterials should produce a composite with very closely spaced regions with the sp^2 and sp^3 hybridized electron shells of carbon atoms. The coexistence of regions with such different electric, thermal, electron, and phonon properties spaced by interfaces of about 1 nm is a unique property. The existence of such interfaces was also confirmed in direct experiments [171].

Consider now the influence of the relation between the shape and sizes of the sp^2/sp^3 regions on TEG efficiency. Based on the results obtained, the optimal carbon TEG nanostructure was proposed, which can be prepared by sintering monodisperse diamond nanostructures of detonation synthesis. The assumed sp^2/sp^3 structures represent an sp^2 matrix doped with sp^3 nanoparticles.

We assume, as usual (see, e.g., [172]), that diamond nanoparticles have the form of polyhedrons completely filling the space, as is demonstrated by the covering of a plane with hexagons with the side L (see Fig. 13). During sintering, in fact, any diamond particle is covered with a graphite-like sp^2 shell of thickness l. These particles, each of them consisting of a diamond-like sp^3 surrounded by an sp^2 layer, form a carbon composite.

Assume that b is the maximum distance over which an electron can be displaced by the phonon drag in the sp^2 region along a straight line without colliding with the sp^3 region boundary. The criterion for the possibility of ballistic drag in the composite is $b > 5$ nm, because the electron mean free path in graphite is ≈ 5 nm (see Section 2.2.2). For the small size of a graphitization region $l \ll L$, the maximum length

over which the electron can be displaced after the absorption of a dragging phonon without colliding with the boundary of a diamond particle is $b \approx L$. Thus, to realize the ballistic phonon drag of electrons in a composite, the composite should be made of small diamonds, i.e., diamond nanoparticles. Monodisperse diamond nanoparticles prepared by detonation synthesis have a size of about 5 nm [112, 113], and therefore the side L of a hexagon in our model slightly exceeds 2.5 nm.

Because the phonon mean free path exceeds L, the electric current I in the composite can appear only when an electron absorbing a phonon moves along a straight line between diamond nanoparticles. This condition is fulfilled when the distance between the sp^3 hybridized nuclei of particles is $L/2$ (see Fig. 13). In this case, the graphite layer thickness is found from the condition $2l = (L/2)\cos(\pi/6)$. This gives $l \geqslant 0.54$ nm. Simple calculations show that the total volumes of the sp^2 and sp^3 carbon hybridization regions are approximately equal. Calculations were performed using the following values of parameters: the diamond lattice constant was 0.357 nm, the distance between graphite layers was 0.335 nm, and the lattice constant in the plane of graphite layers was 0.246 nm. These values in graphite-like and diamond-like structures can be slightly different.

The electric conduction of the sp^2 region is many orders of magnitude higher than that of the sp^3 region, and therefore the current mainly flows in graphite-like sp^2 regions (see Fig. 13). The conductivity of such a region is determined by the electric conduction coefficient of the semimetal and the ratio of the characteristic section of the region to the size in the current flow direction. The size in the current flow direction for a graphite-like layer covering diamond nanoparticles is approximately equal to that in the transverse direction, along the section. It is easy to understand that the ratio of the region area to this size and, therefore, the composite conductivity is directly proportional to the thickness of the sp^2 regions. Thus, the optimal structure will be one in which the thickness of sp^2 regions corresponds to the maximum thickness still allowing the ballistic phonon drag of electrons. At the greater thickness of graphite-like layers, the motion of phonons becomes chaotic, and the thermal emf coefficient drastically decreases. On the other hand, at a smaller thickness of graphite-like layers, the conductivity of the composite decreases.

In a nanocomposite optimal for a TEG, what is important is not only a decrease in the heat conduction caused by the influence of each of the metal/dielectric (sp^2/sp^3) interfaces, but also the influence of interfaces on each other. Consider first a system with two interfaces — planes with coordinates x_1 and x_2, shown in Fig. 14, when a thin graphite-like 'metal' region is located between 'dielectrics' — diamond-like regions. We assume that the dielectric located at the left (Ins 1) is heated.

To find the final thermal resistance r of such a carbon nanostructure, it is necessary to calculate the temperature jump ΔT after the propagation of the thermal flow q through the entire sp^2 region, i.e., the temperature jump at the interface with the coordinate x_2. Figure 14 shows that $\Delta T \approx \Delta T_{\rm rel} = T_{\rm e}(x_2) - T_{\rm ph}(x_2)$. Note that, as in the problem about the thermal resistance of one interface considered in Section 4.2.1, the temperature jump ΔT measured in experiments almost coincides with the one caused by the relaxation equalization of temperatures of the electron ($T_{\rm e}$) and phonon ($T_{\rm ph}$) subsystems. In turn, $T_{\rm e}$ at interfaces almost coincides

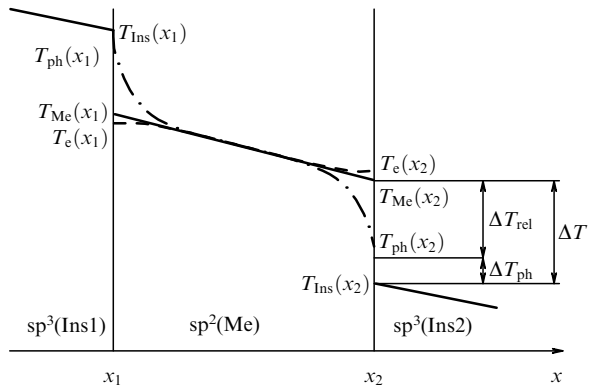

Figure 14. Geometry of the model problem for measuring temperatures T of the electron (dashed line) and phonon (dashed-dotted line) subsystems in the sp^2 region with metal properties (Me) located between sp^3 regions with dielectric properties (Ins). The solid straight line shows the temperature $T_{\rm Me}$, which usually approximates the temperature in the region with metal properties. Temperatures at the boundaries are indicated. ΔT is the temperature jump usually considered in measurements of the heat transfer and its components: temperature jump $\Delta T_{\rm ph}$ of the phonon subsystem and temperature jump $\Delta T_{\rm rel}$ appearing due to heat transfer from the electron subsystem. Other explanations are in the text.

with temperatures $T_{\rm Me}$ of the metal obtained by linear extrapolation.

To solve the problem on the influence of numerous interfaces, it is necessary first to calculate the relaxation thermal resistance in a metal (sp^2) film between two dielectric (sp^3) half-spaces. Figure 14 shows the geometry of the problem.

The formulated problem is a combination of two problems on heat transfer through the metal/dielectric interface considered above (see Fig. 12 and Section 4.2.1). As in the problem of heat transition through one interface, we assume that heat in a metal is transferred only by two subsystems: the electron gas and crystal lattice (phonons), whereas the influence of other subsystems, for example, defects, is insignificant. Therefore, the heat flow in a metal can be written as $q_{\rm e} + q_{\rm ph} = q$. Recall that each subsystem in a metal is characterized by its own heat conduction related to the electron ($\chi_{\rm e}$) and phonon ($\chi_{\rm ph}$) subsystems, and $\chi = \chi_{\rm e} + \chi_{\rm ph}$. The heat propagation in a metal is accompanied by thermal exchange between the subsystems characterized by the coefficient θ.

The solution to the model problem of calculating the relaxation thermal resistance in a metal (sp^2) film between two dielectric (sp^3) layers is considered in detail in [173, 174]. It was found that the temperature of the phonon subsystem in a metal film is distributed as

$$T_{\rm ph} = T_{\rm ph}(x_1) - \frac{q}{\chi}\Lambda\left\{\frac{x}{\Lambda} - \frac{\chi_{\rm e}}{\chi}\frac{\sinh\left[x/\Lambda - (x_2 - x_1)/(2\Lambda)\right]}{\cosh\left[(x_2 - x_1)/(2\Lambda)\right]}\right\},$$

where Λ is the effective length on which the electron and phonon temperatures are equalized (Λ is described by (6), as in the problem with one interface). The boundary thermal resistance also changes due to relaxation of the electron and phonon temperatures, not at one, but at two interfaces:

$$r \approx r_{\rm rel} = \frac{\chi_{\rm e}}{\chi_{\rm ph}\chi}\Lambda\tanh\left(\frac{x_2 - x_1}{2\Lambda}\right).$$

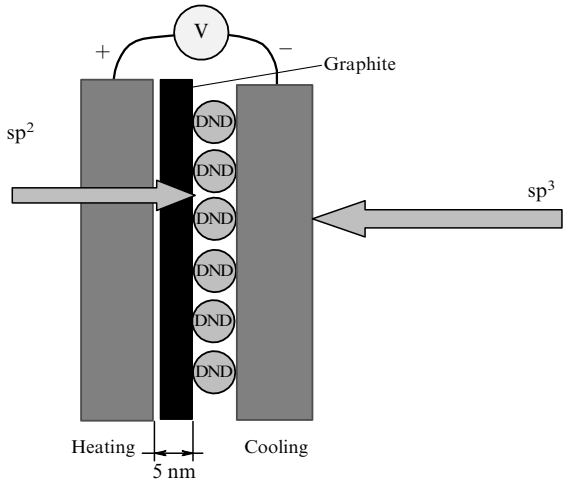

Figure 15. Optimal TEG design according to patent [110]. Along with a graphite-like film 5 nm in thickness and two much thicker diamond-like films, the design contains a matrix with the sp^2 structure with detonation diamond nanoparticles (DND — Detonation Nanodiamond) [114, 115].

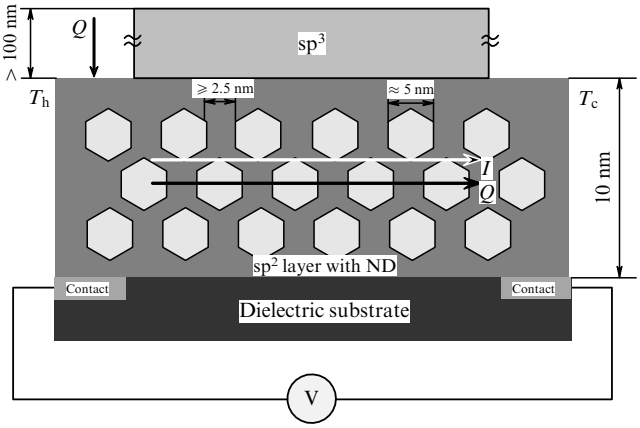

Figure 16. Model of the optimal TEG based on a composite consisting of the matrix sp^2 structure with diamond nanoparticles. T_c and T_h are temperatures of the cooled and heated parts, respectively. The composite contains diamond nanoparticles (ND) ≈ 5 nm in size in a graphite-like matrix — a 10-nm-thick film where the distance between nanoparticles is $\geqslant 2.5$ nm. Other explanations are in the text.

It can be seen that, at large film thicknesses, the relaxation thermal resistance saturates. At small film thicknesses, this resistance is proportional to the film thickness and is independent of the heat transfer between subsystems:

$$r = \frac{\chi_e}{\chi_{ph}\chi}(x_2 - x_1)\,. \tag{8}$$

A TEG prototype considered below (Fig. 15) has numerous interfaces. The heat conduction of this system is calculated using the results obtained above, assuming that the model system (see Fig. 14) is a repeating element in a system with numerous interfaces. We assume that all the layers (sp^2 films) are identical and have the same small thickness $2l$ (see Fig. 13). Because the film thickness in these structures is much smaller than the characteristic temperature-equalization length (7) near one interface, $\Lambda > 30$ nm [173], we will estimate the heat conduction from (8) by disregarding the temperature lowering caused by dissipation in the volume. This can be done for $l \ll \Lambda$. All the sp^3 regions alternating with the sp^2 layers are made of the same material. We assume that sp^3 regions have the same size, $L \approx 4$ nm (see Fig. 13).

One can see from (8) that the heat conduction of the structure under study linearly decreases with the increase in the sp^2 film thickness $l \sim L$, which leads to an increase in the thermoelectric parameter $Z = \gamma^2\sigma/\chi$, where γ is the thermal emf coefficient (Seebeck coefficient), and σ and χ are the electric and heat conduction coefficients of the sp^2 component (the composite matrix). It is important that the heat conduction of the composite decreases due to the heat release at boundaries, and therefore the proportionality between σ and χ according to the Wiedemann–Franz law is absent!

Thus, as the heat conduction decreases, parameter Z increases upon increasing the thickness of graphite-like layers. Of course, the total increase is important, which occurs until ballistic phonon drag exists in the structure. When the optimal film thickness $2l = (L/2)\cos(\pi/6)$ is achieved (see Fig. 13), the heat conduction of χ_c of the structure under study is determined by the thermal resistance $r = 1/\chi_c$, equal in the construction with optimal parameters shown in Fig. 13 to

$$r = \frac{\sqrt{3}}{4\chi}\left(\frac{3\chi}{\chi_d} + \frac{\chi_e}{\chi_{ph}} + 1\right).$$

As shown in Section 5, such a structure provides the maximum thermal emf coefficient of 80 μV K^{-1} compared to composites not having the optimal structure, demonstrating its increase by a factor of 40 for the minimal heat conduction of 5 W m^{-1} K^{-1}, which means a fivefold decrease in the heat conduction. These results were obtained for invariable electric conduction. The combined action of these two effects should result in a three order of magnitude increase in the thermoelectric efficiency parameter Z.

Thermoelectric generators based on the composite with diamond nanoparticles shown schematically in Fig. 16 can be used to build batteries, like TEG batteries based on film structures (see Section 3).

5. Thermoelectric generator based on a composite of an sp^2 matrix structure with diamond nanoparticles

In this section, the properties of TEGs based on composites produced by the sintering of diamond nanoparticles are discussed [7]. At present, it is the sintering method that seems promising for the production of structures (see Fig. 13) with the optimal values of thermal emf, electric, and heat conduction.

The TEG design patented as a useful model [110] is shown in Fig. 15. The TEG model corresponding to the theory developed in Sections 2 and 4 is presented in Fig. 16.

According to the results presented in Sections 2 and 3, to achieve the ballistic phonon drag of electrons, diamond-like sp^3 layers are needed to remove heat from sp^2 regions. The thickness of an sp^2 layer should be of the order of the phonon mean free path. The sp^2 layer itself should be a matrix containing diamond nanoparticles. The sintering produces a composite in which each nanoparticle consists of a diamond-like sp^3 kernel surrounded by the sp^2 layer of the matrix. Such a structure should be as close as possible to the ideal structure calculated in Section 4 (see Fig. 13).

The phonon mean free path in the sp^2 region is estimated as ≈ 5 nm in Section 2.2.2. If the sp^2 region contains diamond nanoparticles about 5 nm in size and the influence of defects on the propagation of phonons can be ignored, then, for an sp^2 region size of 10 nm or even slightly larger (see Fig. 16), the drag of electrons will be mainly determined by ballistic phonons. It is known that long-wavelength acoustic phonons make the main contribution to the drag [175], and electron–phonon interaction at temperatures above 10 K occurs namely due to absorption of such longitudinal acoustic phonons [134].

Thus, the optimal technologically achievable sizes of the model shown in Fig. 16 are the sp^2 layer thickness of about 10–20 nm and the thickness of the sp^3 layer above 100 nm.

The basic requirements for the choice of a thermoelectric functional material are, first, a high thermal emf coefficient and, second, a reduction in the heat conduction without the simultaneous reduction in the electric conduction. Based on the results presented above and taking the most adverse values, we can estimate quantities entering Z such as $\gamma \geqslant 0.1$ V K^{-1}, $\sigma \approx 1$ S m^{-1}, and $\chi \approx 1/r \approx 10$ W m^{-1} K^{-1}. Then, the proposed TEG construction should have the thermoelectric efficiency $ZT \geqslant 1$.

So far, attempts to create the TEG construction shown in Fig. 16 have failed. More specifically, researchers have not been able to create a matrix — an sp^2 film containing faceted diamond nanoparticles 4–5 nm in size and a thickness smaller than 20 nm required to obtain ballistic drag. The high-pressure, high-temperature method was used to produce specks of diamond nanoparticles [137, 176] with a structure similar to that shown in Fig. 13, although not satisfying the optimization conditions presented above, for example, in thickness; also missing is a 'cooler' — an sp^3 film. The heat can be removed from sp^3 regions of only a few particles contacting a high-pressure chamber in which sintering occurs.

Measurements of the heat conduction ($\chi \approx 2$–7 W m^{-1} K^{-1}) and electric conduction ($\sigma \leqslant 0.6$ S m^{-1}) of speck samples obtained at a pressure of 7 GPa and temperature above 1500 K from agglomerates 100–200 nm in size of diamond nanoparticles 4–5 nm in size show that the chosen construction is promising. This is confirmed by the measurements of the thermal emf coefficient of specks presented in Fig. 17.

The thermal emf coefficient in Fig. 17 has a distinct maximum. Because the amount of the sp^2 phase undoubtedly increases with increasing sintering temperature, we can assume that this dependence confirms the conclusion about the existence of the optimal sp^2/sp^3 ratio made in Section 4. The maximum value of the thermal emf coefficient exceeds the minimum value 5 μV K^{-1} for graphite by less than twentyfold, rather than 1000-fold, as expected by comparing the combined efficiency of the phonon drags of electrons with the diffusion mechanism. This is explained by the fact that, as mentioned, the optimal TEG design has not been created.

It seems that a porous structure, which is undoubtedly inherent in a powder before sintering, disappears at pressures of about 7 GPa. This is confirmed, in particular, by measurements of the speck density, which amounts to about 2.8 g cm^{-3}. However, the requirement that at temperatures above 1400 °C the graphitization of the surface of particles 4 nm in size occur at the same depth independent of the size of the initial aggregate and the location of the particle with respect to the agglomerate surface seems not to be fulfilled. The model should also be modified. Clearly, individual particles 4 nm in size will never be arranged so symmetrically as shown in Fig. 13. A principal disadvantage is also the absence of efficient heat removal.

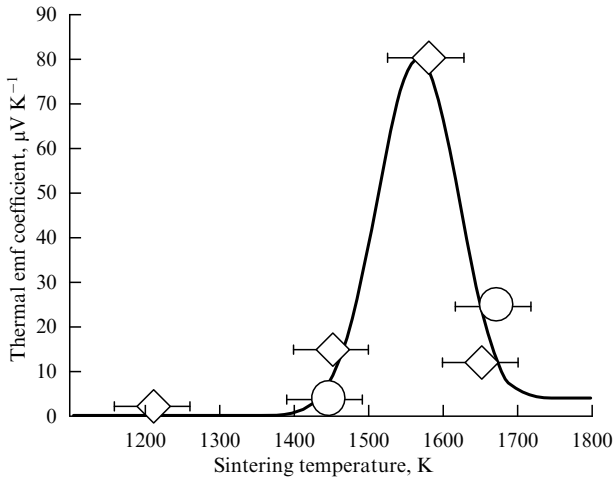

Figure 17. Dependence of the thermal emf coefficient on the sintering temperature. Typical temperature measurement errors are shown for clarity. Diamonds correspond to specks with a 5% mass addition of fullerenes. This addition prevents the sample from spilling. Circles correspond to specks without this addition.

Nevertheless, the experimental result presented in Fig. 17 can be considered promising. In the development of a TEG, it is important to obtain the maximum value of the parameter Z, which is determined not only by the increased thermal emf coefficient but also by the assumed heat conduction coefficient undoubtedly decreasing in the composite under study.

6. Thermal emf of graphene

6.1 Phonon drag of electrons in graphene

The thermal emf of two-dimensional systems has been considered in many studies (see, e.g., [177–187]). However, the thermal emf coefficient of graphene in the mechanism of the phonon drag of electrons was calculated only in [138, 188]. The contribution of the phonon drag of electrons to the thermoelectric current in graphene was studied in [188, 189] based on ideas considered in [1] (see Section 2).

It is known that graphene is a material with strong electron–phonon interaction [190–192]. Therefore, we can expect that the phonon drag will make a considerable contribution to the thermoelectric properties of graphene. The qualitative picture of the phonon drag of electrons in graphene does not differ from the usual one (see [2] or [131]). Graphene can be treated as a semimetal (Fig. 18). However, the quantitative theory and the calculation of the thermal emf coefficient are significantly different.

The phonon drag of electrons at room temperature proved to be insignificant compared to diffusion, but its relative contribution increases with decreasing temperature. The dependence of the drag thermoelectric current on temperature $k_B T$ (below, simply T) and the Fermi energy ε_F fundamentally differs from similar dependences for the diffusion current.

Consider an electron in a state with the wave vector $\mathbf{k}$. As in Section 2.2.3, we can calculate the probability of transition of this electron to a state with the wave vector $\mathbf{k}'$ during the absorption of a phonon with the wave vector $\mathbf{q} = \mathbf{k}' - \mathbf{k}$. A specific feature of graphene is that the electron energy ε near

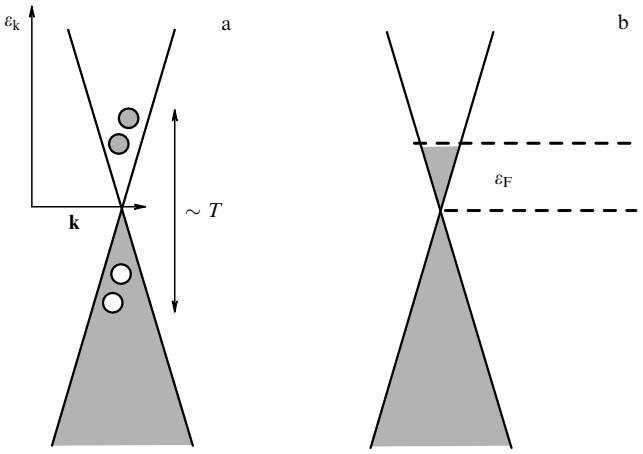

Figure 18. Band structure of graphene upon heating. The thermoelectric effect is possible. Graphene conductivity is similar to that of a graphite-like material, but it has the linear dispersion law $\varepsilon = \hbar v_F k$. (a) Electrons appear in the conduction band due to heating up to temperature T. (b) Fermi level in graphene. The 'Fermi sea' is shown.

the Dirac point (Fig. 18a) is directly proportional to the wave vector: $\varepsilon = \hbar v_F k$. The distribution of phonons with frequency ω_{ph} is described, as usual, by the Bose–Einstein expression $n_{ph}(q)$.

The matrix element in the strong coupling model and the deformation potential approximation were calculated in [189]. The electronic transition probability has the form

$$W = w(\mathbf{k} \to \mathbf{k}')\, n_{ph}(\mathbf{k} - \mathbf{k}')\, \delta\left(\mathbf{k}' - \mathbf{k} \pm \frac{\omega_{ph}(\mathbf{k}' - \mathbf{k})}{v_F}\right),$$

where

$$w(\mathbf{k} \to \mathbf{k}') = \frac{2\pi}{\hbar} \frac{1}{v_F m \omega_{ph}(\mathbf{k}' - \mathbf{k})} \left|D(\mathbf{k} \to \mathbf{k}')\right|^2 \frac{S}{N}.$$

Here, S is the graphene sample area, m is the carbon atom mass, and N is the number of crystal cells in a sample. The quantity w is used in the kinetic equation. Note that the transition probability is obtained proportional to the density of atoms in a graphene crystal.

For small values of the wave vectors of phonons and electrons near Dirac points, we can assume [189, 193] that the direct proportional dependence

$$D(\mathbf{k} \to \mathbf{k}') \sim \varepsilon_a q$$

exists for the matrix element D. One can see from this expression that the modulus of the matrix element is proportional to the modulus of the phonon wave vector. The introduced parameter ε_a should be of the order of the bond energy in the atom. Then, the ratio ε_a/a of the bond energy to the lattice constant gives the estimate of the electron energy gradient in graphene. In the approximation used, the matrix element is independent of the directions of the wave vectors.

6.2 Calculation of the thermal emf coefficient of graphene

6.2.1 Thermoelectric current caused by the phonon drag of electrons in graphene. We will consider the phonon drag of electrons according to the approach presented in [135, Ch. IX, § 10].

We assume that the electron subsystem does not affect the phonon system. We will use the kinetic equation to estimate the influence of the temperature gradient of the phonon distribution in a sample in the relaxation time (τ_{ph}) approximation. Then, the phonon distribution function will obtain, as usual, a small addition,

$$n_{ph}^{(1)}(\mathbf{q}) = \frac{\tau_{ph}(\mathbf{q})}{\hbar q^2}\left(\mathbf{q}\,\frac{\partial T}{\partial \mathbf{r}}\right).$$

To solve the kinetic equation taking into account the absorption of a phonon by an electron and the decay of this pair into an electron and phonon, it is necessary to know the collision integral

$$\left(\frac{\partial}{\partial t} f(\mathbf{k}, \mathbf{r})\right)_{coll} = \left(\frac{\partial}{\partial t} f^{(1)}(\mathbf{k}, \mathbf{r})\right)_{ph}.$$

The collision integral contains the electron distribution function $f(\mathbf{k}, \mathbf{r})$ depending on the wave vector $\mathbf{k}$ and spatial coordinates $\mathbf{r}$. The electron distribution function consists of the Fermi–Dirac function $f^{(0)}$ with energy ε and a small addition $f^{(1)}$. Using expressions for the electronic transition probability during scattering by phonons obtained in Section 6.1.1, we write

$$\left(\frac{\partial}{\partial t} f^{(1)}(\mathbf{k})\right)_{ph} = \int \frac{dq}{4\pi^2} \frac{\partial f^{(0)}}{\partial \varepsilon}\, \hbar\omega_{ph}(q) \times n_{ph}^{(1)}\big(w(\mathbf{k} \to \mathbf{k} + \mathbf{q}) + w(\mathbf{k} + \mathbf{q} \to \mathbf{k})\big)\delta\big(|\mathbf{k} + \mathbf{q}| - |\mathbf{k}|\big).$$

One should bear in mind that transition probabilities w entering these equations correspond to chaotic processes and therefore depend only on the magnitude of the phonon wave vector, but not on its direction.

Below, calculations are performed (see [135, Ch. VII, § 4]) using the phenomenological power dependence of the phonon relaxation time on the wave vector. We have

$$\tau_{ph}(\mathbf{q}) = A q^g,$$

where A is the proportionality coefficient.

We obtain the following expression:

$$\left(\frac{\partial}{\partial t} f^{(1)}(\mathbf{k})\right)_{ph} = \frac{S}{\hbar N} \frac{\varepsilon_a^2 A}{m v_F} \left(\frac{\partial T}{\partial x}\right)\left(\frac{\partial f^{(0)}}{\partial \varepsilon}\right) \times \left[(2k)^{2+g} \cos\theta_k\, \frac{\sqrt{\pi}}{2}\, \frac{\Gamma(3/2 + g/2)}{\Gamma(2 + g/2)}\right].$$

The factor with the gamma function for reasonable exponents g in the dependence of the phonon relaxation time on the wave vector is about unity. It is assumed that the x-axis is directed along the vector $\mathbf{k}$. The expression written above can be represented in the form

$$\left(\frac{\partial}{\partial t} f^{(1)}(\mathbf{k})\right)_{ph} = \left(v_F\, \frac{\mathbf{k}}{k}\, \nabla T\right)\left(\frac{\partial f^{(0)}}{\partial \varepsilon}\right) G_{ph}(k),$$

where the dimensionless function $G_{ph}(k)$ is introduced, which can be found from a comparison with the previous expression.

We can now calculate the thermoelectric current caused by the random phonon drag of electrons.

Let us write the stationary kinetic equation for processes of the absorption of a phonon by an electron and the decay of this pair into an electron and phonon, assuming the presence of the temperature and chemical potential μ gradients and the electric field $\mathbf{E}$. In this case, the phonon collision integral is a part of the coefficient in front of the temperature gradient, while the electron collision integral in the relaxation time $\tau(k)$ approximation remains on the right-hand side. We have

$$\mathbf{v}_k \frac{\partial f^{(0)}}{\partial \varepsilon} \left[\frac{\mu - E - G_{\mathrm{ph}}(k)T}{T} \nabla T - \nabla \mu + e\mathbf{E} \right] = \frac{f^{(1)}(\mathbf{k})}{\tau(\mathbf{k})} . \quad (9)$$

From this, we can find the addition to the distribution function caused by the phonon drag of electrons:

$$f_{\mathrm{ph}}^{(1)} = (\mathbf{v}_k \nabla T) \frac{\partial f^{(0)}}{\partial \varepsilon} G_{\mathrm{ph}}(k)\tau(k) .$$

The rest of the terms on the left-hand side of the kinetic equation determine the addition to the distribution function caused by the interaction of only electrons. This addition will be considered later.

The general expression [131] for the current density produced by electrons with velocities $\mathbf{v}_k$ along the $\mathbf{k}$ direction in two-dimensional graphene has the form

$$\mathbf{j} = e \frac{1}{\pi^2} \int \mathrm{d}^2 k \, f^{(1)}(\mathbf{k}) \mathbf{v}_k .$$

Let us introduce a phenomenological power dependence of the electron relaxation time on the modulus of their wave vector or energy:

$$\tau(k) = Bk^b = \tilde{B}\varepsilon^b ,$$

where B and $\tilde{B}$ are coefficients.

Now, it is necessary to discuss the position of the Fermi level in the system (Fig. 18b).

We assume that the 'Fermi sea' submerges the linking place of cones at the Dirac point and that the Fermi energy ε_{F} measured from the cone linking point proves to be much higher than the temperature, which corresponds to the case of a strong degeneracy of the electron gas. Then, transfer processes contain only the contribution of electrons with energy near ε_{F}.

The expression for the relaxation time $\tau(k_{\mathrm{F}})$ of electrons with the Fermi energy is similar to the expression (see [135], Ch. IX, § 7, formula (7.8)) for the conductivity of metals. Then, as is known, the temperature correction to the integral will be proportional to T^2. The electric conductivity coefficient in the expression for current has the form

$$\sigma = \frac{e^2 v_{\mathrm{F}}}{2\pi\hbar} \tau(k_{\mathrm{F}}) k_{\mathrm{F}} .$$

The electric conductivity coefficient in graphene, which is a two-dimensional system, has the dimensionality S, rather than S m^{-1}, as in a three-dimensional system. Similar changes in the dimensionality are also present for other quantities characterizing graphene. The final expression for current produced by the phonon drag of electrons in graphene has the form

$$j_{\mathrm{ph}} = \frac{\sigma}{e} \frac{S}{N} \frac{\varepsilon_{\mathrm{a}}^2 \tau_{\mathrm{ph}}(k_{\mathrm{F}})}{m\hbar v_{\mathrm{F}}^2} \frac{\partial T}{\partial r} k_{\mathrm{F}}^2 \left[2^{1+g} \frac{1}{\sqrt{\pi}} \frac{\Gamma(3/2 + g/2)}{\Gamma(2 + g/2)} \right] . \quad (10)$$

6.2.2 Thermoelectric current caused by the diffusion of electrons in graphene. The temperature dependence of the chemical potential in graphene has the form

$$\mu = \varepsilon_{\mathrm{F}} \left(1 - \frac{\pi^2}{6} \left(\frac{T}{\varepsilon_{\mathrm{F}}} \right)^2 \right) .$$

This expression is similar to the corresponding one for the chemical potential of the electron gas (see [151]), except for the doubled factor in front of the temperature squared, which is due to the two-dimensionality of graphene.

We now use kinetic equation (9) in the relaxation time approximation, but without the phonon contribution. By substituting the expression for chemical potential into (9), we obtain the correction to the electronic distribution function:

$$f^{(1)}(\mathbf{k}) = \tau(\varepsilon_k) \frac{\partial f^0}{\partial \varepsilon} \left(\frac{\varepsilon_k - \mu}{T} - \frac{\pi^2}{3} \frac{T}{\mu} \right) \frac{v_{\mathrm{F}}}{k} (\mathbf{k} \nabla T) .$$

After integration with an arbitrary parameter b, the expression for the current produced by diffusion of electrons in graphene will have the form

$$\mathbf{j} = e \nabla T \frac{\pi}{3\hbar^2} T \tau(k_{\mathrm{F}})(b - 0.5) . \quad (11)$$

6.2.3 Thermal emf coefficient of graphene. Obviously, expressions (10) and (11) for currents contain many identical quantities. First of all, they are the electron relaxation time and the temperature gradient, and also the electron charge and Planck's constant squared. The ratio of currents caused by various mechanisms is

$$\frac{j_{\mathrm{ph}}}{j} = \frac{1}{T} \frac{S}{N} \frac{\varepsilon_{\mathrm{a}}^2 \tau_{\mathrm{ph}}(k_{\mathrm{F}})}{m v_{\mathrm{F}}} k_{\mathrm{F}}^3 C_j ,$$

where C_j is the dimensionless coefficient around unity for reasonable values of phenomenological exponents b and g.

Further estimates can be conveniently performed by expressing the Fermi momentum $\hbar k_{\mathrm{F}}$ in terms of the lattice constant a, the Fermi energy ε_{F}, and the atomic bond energy ε_{a}. Obviously,

$$k_{\mathrm{F}} = \frac{\pi}{a} \frac{\varepsilon_{\mathrm{F}}}{\varepsilon_{\mathrm{a}}} .$$

The ratio S/N is also expressed via the lattice constant. As a result, the ratio of current is written in the form

$$\frac{j_{\mathrm{ph}}}{j} = \frac{\varepsilon_{\mathrm{F}}}{k_{\mathrm{B}} T} \frac{\varepsilon_{\mathrm{F}}}{\varepsilon_{\mathrm{a}}} \frac{\varepsilon_{\mathrm{F}}}{\varepsilon_{\mathrm{c}}} \pi^3 C_j . \quad (12)$$

This expression contains one more quantity,

$$\varepsilon_{\mathrm{c}} = \frac{m v_{\mathrm{F}} a}{\tau_{\mathrm{ph}}(k_{\mathrm{F}})} ,$$

with the dimensionality of energy characterizing the electron–phonon interaction energy.

The Fermi energy ε_{F} in graphene can be estimated as 0.1 eV and the atomic bond energy ε_{a} as 10 eV. This gives the product of the first two cofactors at room temperature in (12) of about 0.01. The relation between the classical diffusion current and the drag thermoelectric current in graphene is determined by energy ε_{c}. The unknown quantity is the

phonon relaxation time only. The same relaxation time also characterizes the heat conduction of graphene, because it determines the phonon flow with the presence of the temperature gradient.

Various mechanisms determining the relaxation time of a phonon system are analyzed in paper [194] explaining the heat conduction of graphene samples. In this paper, the theory was compared with experiments in the temperature range of 10–1000 K. One can assume that the experimental setup and graphene samples used in [194] can also be applied for measurements of the thermoelectric current, and therefore the values of the constants are taken from this paper.

Three relaxation mechanisms of a phonon system exist. The first mechanism is related to anharmonic vibrations in the interaction of atoms in a crystal lattice and correspondingly to three-phonon processes. However, anharmonic corrections become important only for large amplitude displacements, which corresponds to the large occupation density of the phonon subsystem. This takes place only at temperatures above 1000 K, greatly exceeding room temperature. The theory of the phonon drag of electrons is developed for considerably lower temperatures, and therefore three-photon processes are not considered here.

The second mechanism is the scattering of phonons by point defects. The phonon drag effect substantially depends on the relaxation time of phonons with the wave vector coinciding with the wave vector of electrons with energy ε_F. The relaxation time τ_{ph}^{d} is described by the expression (see [195, 196])

$$\frac{1}{\tau_{ph}^{d}(k_F)} = C_d c \frac{\varepsilon_F}{\varepsilon_a} \omega_{max} ,$$

where C_d is a coefficient of about 10 depending on the defect type, $c \approx 10^{-6}$ is the relative concentration of defects, and $\omega_{max} \approx 3 \times 10^{-14}$ s^{-1} is the maximum phonon frequency. For the data presented in [195], the relaxation time in graphene in this mechanism is $10^{-3} - 10^{-4}$ s.

Finally, the third mechanism is the scattering of phonons by sample boundaries — graphene lobes. In this case, the relaxation time τ_{ph}^{b} corresponds to the phonon transit time over the entire sample. The size of graphene lobes used in [195] was 1–10 μm. The phonon velocity (sound velocity) is 10^3 m s^{-1}. These values give a time of about 1–10 ns. The relaxation time of the phonon system is determined by the smaller time — the time of scattering by sample edges — and is about 1 ns.

The estimated relaxation time of the phonon subsystem of graphene allows us to estimate the electron–phonon interaction energy as $\varepsilon_c \approx 0.01$ eV. This means that the ratio of the current caused by the phonon drag of electrons and the classical diffusion current proves to be about unity at room temperature.

We can now estimate the thermoelectric current in graphene caused by the phonon drag. Let us rewrite expression (10) in the form

$$j_{ph} = \sigma \gamma k_B \frac{dT}{dx} ,$$

where the thermal emf coefficient of graphene related to the phonon drag of electrons can be estimated as $\gamma \approx 10 - 80$ μV K^{-1}. This is the main result of this section. Figure 19 presents the thermal emf coefficients due to the phonon drag of electrons and the diffusion mechanism as functions of the Fermi energy ε_F at room temperature. One can see that the thermal emf coefficient of graphene produced by the phonon drag of electrons greatly exceeds the thermal emf coefficient of graphite equal to 4 μV K^{-1}.

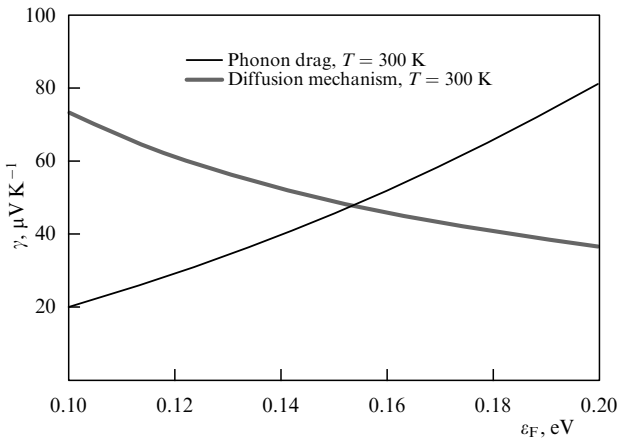

Figure 19. Contributions to the thermal emf coefficient γ graphene as functions of the Fermi energy ε_F at room temperature. The thin line is the contribution of the phonon drag of electrons, and the thick line is the contribution of the diffusion mechanism.

Note that the phonon energy is approximately two orders of magnitude lower than the energy of electrons with the same value of the wave vector. This is explained by the fact that the phonon velocity (sound velocity) greatly exceeds the electron velocity (Fermi velocity). To observe the drag effect, phonons with a wave vector of the order of k_F should be excited, which therefore have an energy of ~ 0.001 eV. In fact, this is the limit of the applicability of this theory over temperature from below, ~ 10 K. At higher temperatures, the phonon drag effect should make the main contribution to the thermoelectricity. Because the drag current is proportional to the Fermi energy in the third power, according to expression (12), we can assume that the contribution of the drag current to the total current will increase with increasing Fermi energy. The phonon drag effect will also increase as the size of graphene lobes increases.

7. Thermoelectric generator based on an sp^2 region graphene matrix composite

Unfortunately, a graphene-based TEG has not been created so far. Graphene and its composites — graphene lobes in a polystyrene matrix — were studied in papers [197–199] and [200–202], respectively. Graphene films on silicon were investigated as well [203]. The aim of all these papers is to learn to place graphene films conveniently to create a TEG.

Based on considerations presented in Sections 2, 4, and 6, we can assume that TEGs based on an sp^2 region graphene lobe composite will have the best parameters (Fig. 20).

Figure 20 presents a graphene-based TEG model similar to that with diamond nanoparticles shown in Fig. 16. An sp^3 layer is prepared, which is covered with an sp^2 matrix layer with graphene lobes. Of course, it is possible to prepare a structure with a substrate covered with an sp^2 matrix layer with graphene lobes and an sp^3 layer deposited above. Possibly, a TEG battery will also be created (see Section 4). A graphene composite should use both effects discussed above, namely, a high thermal emf and low heat conduction.

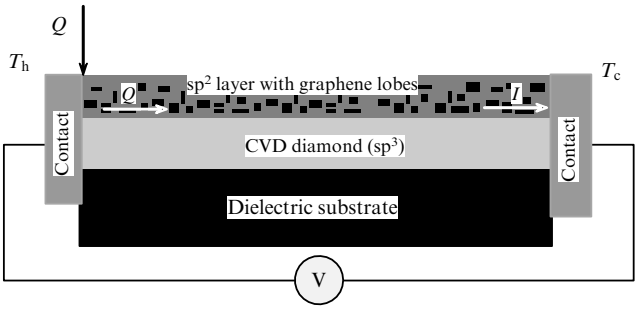

Figure 20. Optimal TEG design based on the matrix sp^2 structure with graphene lobes. T_c and T_h are temperatures of the cooled and heated parts. The composite should be a structure containing a speck of graphene lobes $\approx 100 \times 100$ nm in size in a graphite-like matrix with lobes spaced $\geqslant 25$ nm apart.

8. Conclusions. Path to a thermoelectric generator with record parameters

Let us compare TEGs proposed at present (see [116, Ch. 11]) and TEGs based on carbon film structures.

The commercial production of semiconductors resulted in the development of TEGs consisting of semiconducting thermoelements in series in an electric circuit, each of them being formed by two branches made of a semiconductor with p- and n-type conductivities, respectively.

It is known [204] that the Bi_2Te_3 melt has the highest thermoelectric efficiency ($Z \approx 0.003$ K^{-1}) at room temperature among homogeneous materials. The highest efficiency Z is achieved because, along with the usual diffusion mechanism of the redistribution of electrons between hot and cold regions in conductors, the much more efficient mechanism of drag of electrons by a thermal flow — phonons — is possible, which is known as the Gurevich effect [2]. The phonon flow drags electrons toward the cold end of a sample, making a contribution to the thermal emf coefficient. In doped bismuth, a Bi_2Te_3 semimetal, this effect determines the total thermal emf coefficient and the record thermoelectric parameter mentioned above. Note that the authors of paper [204] do not mention the mechanism of phonon drag of electrons in the explanation of the thermoelectric effect.

A thermoelectric element exists (see patent [205]) containing bismuth (or a melt with bismuth, bismuth in other metals, and mixtures of these materials, possibly containing some additions) as an additional material placed into extended, parallel-oriented pores of the main porous material with pores 5–15 nm in size. The main material is unoxidized porous aluminum, porous glass, or porous silica gel in the volume form. Electric contacts are connected to the end surfaces of the additional material in pores of the main material.

The record high value of parameter $Z = 0.08$ K^{-1} at 77 K achieved in such a thermoelectric element is at present not yet sufficient for many applications; in addition, the thermoelectric element has a relatively low efficiency and cannot satisfy ecological requirements. Note that the ballistic phonon drag of electrons undoubtedly takes place in this element, but the authors of patent [205] do not mention this mechanism of the thermoelectric effect (see, e.g., [170]).

A thermoelectric material developed based on carbon nanostructures (see Section 5) has a higher Seebeck coefficient than in traditional semiconductors and, correspondingly, a higher power conversion coefficient, as well as high shock resistance, high temperature deformation resistance, and a higher bending ability. Carbon is a much more environmentally friendly material than bismuth. However, the thermoelectric efficiency Z of TEGs based on carbon nanostructures is also so far insufficient for many technical applications.

Based on carbon nanostructures, two patents for the invention (see [109, 110]) and a patent for the useful model [108] have been obtained to date. The value of parameter $Z \approx 0.01$ K^{-1} was achieved at room temperature due to the ballistic phonon drag of electrons (see Section 3) and independently due to a decrease in the heat conduction caused by a great amount of graphite-like and diamond-like materials. Undoubtedly, the combined action of these two mechanisms will increase the parameter Z to 0.1 K^{-1}.

All the constructions proposed use a carbon material with the sp^3 hybridization of atomic bonds or carbon atoms or graphene as the main material of the thermoelectric element, while a carbon material with the sp^2 hybridization is used as an additional material. Thermoelectric elements based on carbon nanostructures obviously satisfy the ecological requirements and also ensure the miniaturization of the device because of the nanometer size of the additional material and the smaller than micrometer size of the main material. This allows one to build mini batteries from such thermoelements satisfying the requirements of users.

In this paper, a review study of the thermoelectric efficiency of carbon nanomaterials consisting of graphite-like and diamond-like regions with the sp^3 and sp^2 hybridization of carbon atoms is performed. The coexistence of regions with absolutely different electric and thermal properties, such as diamond and graphite, at such small distances from each other is a unique property inherent only in such structures. Based on this study, the recent theory of heat transfer through the diamond-like–graphite-like interface and the theory of ballistic phonon drag of electrons are applied to the calculation of the efficiency of a thermoelectric element.

The measurement of the heat conduction and electric conduction of carbon nanomaterials proposed for use in thermoelectric elements in the form of films showed that the TEG designs proposed here are promising.

Measurements of the characteristics of specks of carbon nanomaterials intended for a thermoelectric element show that, in the case of optimal sizes of the sp^3 and sp^2 layers and composites based on the sp^2 matrix with diamond nanoparticles 4 nm in size, the production of TEGs with a thermoelectric efficiency of a few units is quite possible.

Thus, the specific features of the electron–phonon interaction in carbon nanostructures are manifested not only in the field emission [206] due to the unique properties of these structures but also in the thermoelectric effect.

Acknowledgments. The author thanks A Ya Vul' for his attention to this study. His participation was especially important at the first stages of the study. The author also thanks Dieter Gruen for pointing out the importance of the drag effect in thermoelectric phenomena, A P Meilakhs and S V Konyakhin for their collaboration in the development of the theory, and F M Shakhov, M K Rabchinskii, and V G Golubev's group for their participation in experiments. The author thanks A V Arkhipov for his participation in the selection of sources, N I Aleksandrov for his help in the preparation of figures, and G I Dmitrieva and N F Nechaeva for their technical assistance.

References

1. Eidelman E D, Vul' A Ya *J. Phys. Condens. Matter* **19** 266210 (2007)
2. Gurevich L E *J. Phys. USSR* **9** 4 (1946); *Zh. Eksp. Teor. Fiz.* **16** 193 (1946)
3. Chen G *Nanoscale Energy Transport and Conversion*: *a Parallel Treatment of Electrons, Molecules, Phonons, and Photons* (Oxford: Oxford Univ. Press, 2005)
4. Zhang Z M *Nano/Microscale Heat Transfer* (New York: McGraw-Hill, 2007)
5. Chen G *Phys. Rev. Lett.* **86** 2297 (2001)
6. Chen G *J. Heat Transfer* **124** 320 (2002)
7. Eidelman E D et al. *J. Phys. D* **50** 464007 (2017)
8. Nikolić B, Allen P B *Phys. Rev. B* **60** 3963 (1999)
9. Chen G *Phys. Rev. B* **57** 14958 (1998)
10. Sharvin Yu V *Sov. Phys. JETP* **21** 655 (1965); *Zh. Eksp. Teor. Fiz.* **48** 984 (1965)
11. Wexler G *Proc. Phys. Soc. Lond.* **89** 927 (1966)
12. Cola B, Xu J, Fisher T S *Int. J. Heat Mass Transfer* **52** 3490 (2009)
13. Prasher R, Tong T, Majumdar A *Appl. Phys. Lett.* **91** 143119 (2007)
14. Prasher R *Phys. Rev. B* **74** 165413 (2006)
15. Saha S K, Shi L *J. Appl. Phys.* **101** 074304 (2007)
16. Prasher R *Nano Lett.* **5** 2155 (2005)
17. Kim W, Majumdar A *J. Appl. Phys.* **99** 084306 (2006)
18. Kim W et al. *Phys. Rev. Lett.* **96** 045901 (2006)
19. Prasher R S, Phelan P E *J. Appl. Phys.* **100** 063538 (2006)
20. Prasher R *J. Appl. Phys.* **100** 064302 (2006)
21. Bahadur V et al. *J. Heat Transfer* **127** 664 (2005)
22. Li D et al. *Appl. Phys. Lett.* **83** 2934 (2003)
23. Lu W, Komvopoulos K *Appl. Phys. Lett.* **82** 2437 (2003)
24. Yu C et al., in *Proc. of the ASME Summer Heat Transfer Conf., San Francisco, CA, 2005* (Little Falls, NJ: ASME) paper No. HT2005–72320, https://doi.org/10.1115/HT2005-72320
25. Wilson O M et al. *Phys. Rev. B* **66** 224301 (2002)
26. Huxtable S T et al. *Nat. Mater.* **2** 731 (2003)
27. Majumdar A, Reddy P *Appl. Phys. Lett.* **84** 4768 (2004)
28. Schwab K et al. *Nature* **404** 974 (2000)
29. Mingo N, Broido D A *Phys. Rev. Lett.* **95** 096105 (2005)
30. Santamore D H, Cross M C *Phys. Rev. B* **63** 184306 (2001)
31. Chang C-M, Geller M R *Phys. Rev. B* **71** 125304 (2005)
32. Prasher R, Tong T, Majumdar A *Nano Lett.* **8** 99 (2008)
33. Milton G W *Theory of Composites* (Cambridge: Cambridge Univ. Press, 2002)
34. Batchelor G K *Annu. Rev. Fluid Mech.* **6** 227 (1974)
35. Prasher R S et al. *J. Heat Transfer* **125** 1170 (2003)
36. Torquato S *Appl. Mech. Rev.* **44** (2) 37 (1991)
37. Rogach A L et al. *Adv. Funct. Mater.* **12** 653 (2002)
38. Chen G, Yang B, Liu W "Engineering nanostructures for energy conversion", in *Heat Transfer and Fluid Flow in Microscale and Nanoscale Structures* (Eds M Faghri, B Sundén) (Southampton: WIT, 2004)
39. Suzdalev I P *Nanotekhnologiya*: *Fiziko-khimiya Nanoklasterov, Nanostruktur i Nanomaterialov* (Nanotechnology: Physical Chemistry of Nanoclusters, Nanostructures and Nanomaterials) 2nd ed. corr. (Moscow: Librokom, 2009)
40. Moniruzzaman M, Winey K I *Macromolecules* **39** 5194 (2006)
41. Weber E "Development and modeling of thermally conductive polymer/carbon composites", Ph.D. Thesis (Houghton, MI: Michigan Technological Univ., 2001)
42. Karayacoubian P "Effective thermal conductivity of composite fluidic thermal interface materials", Thesis of Master of Applied Science (Waterloo, ON: Univ. of Waterloo, 2006)
43. Bhushah B (Ed.) *Springer Handbook of Nanotechnology* 2nd ed. (Berlin: Springer Science + Business Media, 2007)
44. Rowe D M (Ed.) *CRC Handbook of Thermoelectrics*: *Macro to Nano* (Boca Raton, FL: CRC Press, 2005)
45. Dresselhaus M et al. *Adv. Mater.* **19** 1043 (2007)
46. Koumoto K, Terasaki I, Funahashi R *MRS Bull.* **31** 206 (2006)
47. Hicks L D, Dresselhaus M S *Phys. Rev. B* **47** 16631(R) (1993)
48. Hicks L D, Dresselhaus M S *Phys. Rev. B* **47** 12727 (1993)
49. Friedman L *J. Phys. C* **17** 3999 (1984)
50. Tao Z, Friedman L *J. Phys. C* **18** L455 (1985)
51. Vashaee D, Shakouri A *Phys. Rev. Lett.* **92** 106103 (2004)
52. Mahan G D, Woods L M *Phys. Rev. Lett.* **80** 4061 (1998)
53. Shakouri A, Bowers J E *Appl. Phys. Lett.* **71** 1234 (1997)
54. Zide J M O et al. *Phys. Rev. B* **74** 205335 (2006)
55. Scherrer H, Scherrer S, in *Thermoelectrics Handbook*: *Macro to Nano* (Ed. D M Rowe) (Boca Raton, FL: CRC Press, 2006) Ch. 27
56. Kutasov V, Lukyanova L, Vedernikov M, in *Thermoelectrics Handbook*: *Macro to Nano* (Ed. D M Rowe) (Boca Raton, FL: CRC. Taylor and Francis, 2006) Ch. 37
57. Kuznetsov V L et al. *J. Mater. Sci.* **37** 2893 (2002)
58. Yao T *Appl. Phys. Lett.* **51** 1798 (1987)
59. Touzelbaev M N et al. *J. Appl. Phys.* **90** 763 (2001)
60. Caylor J C et al. *Appl. Phys. Lett.* **87** 023105 (2005)
61. Beyer H et al. *Physica E* **13** 965 (2002)
62. Kim W et al. *Appl. Phys. Lett.* **88** 242107 (2006)
63. Kim W et al. *Phys. Rev. Lett.* **96** 045901 (2006)
64. Chen G *Semicond. Semimet.* **71** 203 (2001)
65. Yang R, Chen G *Phys. Rev. B* **69** 195316 (2004)
66. Poudel B et al. *Science* **320** 634 (2008)
67. Hsu K F et al. *Science* **303** 818 (2004)
68. Fluerial J, Caillat T, Borshchevsky A, in *Proc. of the 13th Intern. Conf. on Thermoelectrics, Kansas City, MO, 30 August – 1 September, 1994* (New York: AIP, 1995) p. 40
69. Lan Y et al. *Nano Lett.* **9** 1419 (2009)
70. Bux S K et al. *Adv. Funct. Mater.* **19** 2445 (2009)
71. Mingo N et al. *Nano Lett.* **9** 711 (2009)
72. Minnich A J et al. *Phys. Rev. B* **80** 155327 (2009)
73. Wang X et al. *Appl. Phys. Lett.* **93** 193121 (2008)
74. Joshi G et al. *Nano Lett.* **8** 4670 (2008)
75. Ma Y et al. *Nano Lett.* **8** 2580 (2008)
76. Ghosh S et al. *New J. Phys.* **11** 095012 (2009)
77. Balandin A A et al. *Nano Lett.* **8** 902 (2008)
78. Nika D L et al. *Phys. Rev. B* **79** 155413 (2009)
79. Lan J et al. *Phys. Rev. B* **79** 115401 (2009)
80. González J, Perfetto E *New J. Phys.* **11** 095015 (2009)
81. Zeng G et al. *Appl. Phys. Lett.* **91** 263510 (2007)
82. Mahajan R, Chiu C, Chrysler G *Proc. IEEE* **94** 1476 (2006)
83. Prasher R et al. *Intel Tech. J.* **9** 285 (2005)
84. Semenyuk V, in *Thermoelectrics Handbook*: *Macro to Nano* (Ed. D M Rowe) (Boca Raton, FL: CRC Press, 2006) Ch. 58–1–58–20
85. Sanders G H W, Manz A *Trends Anal. Chem.* **19** 364 (2000)
86. Chowdhury I et al. *Nat. Nanotechnol.* **4** 235 (2009)
87. Meysenc L, Jylhakallio M, Barbosa P *IEEE Trans. Power Electron* **20** 687 (2005)
88. Majumdar A *Nat. Nanotechnol.* **4** 214 (2009)
89. Satyala N, Norouzzadeh P, Vashaee D, in *Nanoscale Thermoelectrics* (Eds X Wang, Z M Wang) (Cham: Springer Intern. Publ., 2014) p. 93
90. Crabtree G, Lewis N *Phys. Today* **60** (3) 37 (2007)
91. Lim J et al. *Adv. Mater.* **17** 1488 (2005)
92. Fukutani K, Singh R, Shakouri A *Thermal Transient Characterization of Packaged Thin Film Microcoolers, Nice, Cote d'Azur, France, 27–29 September, 2006*
93. Ziman J M *Principles of the Theory of Solids* (Cambridge: Univ. Press, 1964); Translated into Russian: *Printsipy Teorii Tverdogo Tela* (Moscow: Mir, 1975)
94. Ziman J M *Electrons and Phonons*; *the Theory of Transport Phenomena in Solid* (Oxford: Clarendon Press, 1960); Translated into Russian: *Elektrony i Fonony* (Moscow: IL, 1962)
95. Landau L D, Lifshitz E M *Electrodynamics of Continuous Media* (Oxford: Pergamon Press, 1984); Translated from Russian: *Elektrodinamika Sploshnykh Sred* (Moscow: Nauka, 1982)
96. Nolas G et al. *Principles of Thermoelectrics*: *Basics and New Materials Development* (Berlin: Springer-Verlag, 2001)
97. Goldsmid H *Thermoelectric Refrigeration* (New York: Plenum Press, 1964)
98. Mahan G, Sales B, Sharp J *Phys. Today* **50** (3) 42 (1997)
99. Abelson R, in *Thermoelectrics Handbook*: *Macro to Nano* (Ed. D M Rowe) (Boca Raton, FL: CRC Press, 2006) Ch. 56, p. 1
100. Vining et al., in *Thermoelectrics Handbook*: *Macro to Nano* (Ed. D M Rowe) (Boca Raton, FL: CRC Press, 2005) A1
101. Sharp J et al. *Principles of Thermoelectrics*: *Basics and New Materials Development* (Berlin: Springer-Verlag, 2001)

102. Vining C, in *Proc. of the European Conf. on Thermoelectrics ECT, Odessa, Ukraine, September 10–12, 2007* (2007) p. 1
103. Bell L E *Science* **321** 1457 (2008)
104. Bahk J, Shakouri A "Electron transport engineering by nanostructures for efficient thermoelectrics", in *Nanoscale Thermoelectrics* (Eds X Wang, Z Wang) (Chur: Springer Intern. Publ., 2014) p. 41
105. Yang R, Chen G *Mater. Integration* **18** 31 (2012)
106. Ioffe A F *Semiconductor Thermoelements and Thermoelectric Cooling* (London: Infosearch Ltd., 1957)
107. Tritt T, Böttner H, Chen L *MRS Bull.* **33** 366 (2008)
108. Eidelman E D, Meilakhs A P, Vul' A Ya "Termoelektricheskii element" ("Thermoelectric element"), Patent for the useful model no. 180604, Application no. 2017143948. Priority of the model of December 14, 2017. The state registration date in the State Register of Useful Models of the Russian Federation June 19, 2018. Patent owner: Federal State Budget Scientific Institution Ioffe Physical-Technical Institute, RAS (RU). Published 19.06.2018. Bull. no. 17
109. Eidelman E D, Shakhov F M, Vul' A Ya "Termoelektricheskii element" ("Thermoelectric element"), Patent for invention no. 2628676, Application no. 2016146445. Priority of invention of November 25, 2016. The state registration date in the State Register of Inventions of the Russian Federation August 21, 2017. Patent owner: Federal State Budget Scientific Institution Ioffe Physical-Technical Institute, RAS (RU)
110. Vul' A Ya, Eidelman E D "Termoelektricheskii element" ("Thermoelectric element"), Patent for invention no. 2376681; Application no. 2008140273. Priority of invention of October 6, 2008. Decision to grant a patent for invention of August 21, 2009. Registered in the State Register of Inventions of the Russian Federation on December 20, 2009. Patent owner: Ioffe Physical-Technical Institute, RAS (RU)
111. Vul' A Ya, Eidelman E D, Dideikin A T, in *Synthesis, Properties and Applications of Ultrananocrystalline Diamond* (NATO Scientific Ser., Ser. II Mathematics, Physics and Chemistry, Vol. 192, Eds D Gruen et al.) (Berlin: Springer, 2003) p. 383
112. Aleksenskiy A E, Eydelman E D, Vul' A Ya *Nanosci. Nanotechnol. Lett.* **3** 68 (2011)
113. Williams O A et al. *ACS Nano* **4** 4824 (2010)
114. Dideikin A T et al. *Tech. Phys.* **55** 1378 (2010); *Zh. Tekh. Fiz.* **80** (9) 146 (2010)
115. Dideykin A et al. *Diamond Relat. Mater.* **20** 105 (2011)
116. Dmitriev A S *Vvedenie v Nanoteplofiziku* (Introduction to Nanothermophysics) (Ser. Nanotechnologies) (Moscow: BINOM. Lab. Znanii, 2015)
117. Ashcroft N W, Mermin N D *Solid State Physics* (New York: Holt, Rinehart and Winston, 1976); Translated into Russian: *Fizika Tverdogo Tela* (Moscow: Mir, 1979)
118. *15th European Conf. on Thermoelectrics (ECT), Padua, Italy, 25–27 September, 2017*; *Mater. Today Proc.* **8** 2214 (2019)
119. *The XVI Interstate Conf. "Thermoelectrics and their Applications-2018" (ISCTA 2018), St. Petersburg, Russia, 8–12 October, 2018*
120. Humphrey T E, Linke H *Phys. Rev. Lett.* **94** 0966011 (2005)
121. Humphrey T E, O'Dwyer M F, Linke H *J. Phys. D* **38** 2051 (2005)
122. O'Dwyer M F et al. *Phys. Rev. B* **72** 205330 (2005)
123. O'Dwyer M F, Humphery T E, Linke H *Nanotechnology* **17** S338 (2006)
124. O'Dwyer M F et al. *J. Phys. D Appl. Phys.* **39** 4153 (2006)
125. Vinogradov A Ya et al. *Semiconductors* **52** 914 (2018); *Fiz. Tekh. Poluprovodn.* **52** 775 (2018)
126. Rabchinskii M K et al. *Tech. Phys. Lett.* **45** 339 (2019); *Pis'ma Zh. Tekh. Fiz.* **45** (7) 33 (2019)
127. Grudinkin S A et al. *Nanotechnology* **27** 395606 (2016)
128. Gurevich L E *Osnovy Fizicheskoi Kinetiki* (Fundamentals of Physical Kinetics) (Leningrad–Moscow: Gostekhteoretizdat, 1940)
129. Sommerfeld A, Bethe H A *Handbuch der Physik* Vol. 24 (Berlin: Springer-Verlag, 1933) p. 333; Translated into Russian: *Elektronnaya Teoriya Metallov* (Leningrad – Moscow, 1938)
130. Stil'bans L S *Fizika Poluprovodnikov* (Physics of Semiconductors) (Moscow: Sov. Radio, 1967)
131. Lifshitz E M, Pitaevskii L P *Physical Kinetics* (Oxford: Pergamon Press, 1981); Translated from Russian: *Fizicheskaya Kinetika* (Moscow: Nauka, 1989)
132. Dideykin A T, Eidelman E D, Vul' A Ya *Solid State Commun.* **126** 495 (2003)
133. Landau L D, Lifshitz E M *Quantum Mechanics. Non-Relativistic Theory* (Oxford: Pergamon Press, 1977); Translated from Russian: *Kvantovaya Mekhanika. Nerelyativistskaya Teoriya* (Moscow: Nauka, 1989)
134. Zylbersztein A *J. Phys.* **33** (Suppl. C4) 85 (1972); Translated into Russian: in *Fizika Fononov Bol'shikh Energii* (Physics of High-Energy Phonons) (Ser. Solid State Physics News, Issue 5) (Moscow: Mir, 1976) p. 101
135. Anselm A *Introduction to Semiconductor Theory* (Englewood Cilffs, NJ: Prentice-Hall, 1981); Translated from Russian: *Vvedenie v Teoriyu Poluprovodnikov* (Moscow: Nauka, 1978)
136. Narayanamurti V et al. *Phys. Rev. Lett.* **43** 2012 (1979)
137. Kidalov S V et al. *Diamond Relat. Mater.* **19** 976 (2010)
138. Kubakaddi S S, Bhargavi K S *Phys. Rev. B* **82** 155410 (2010)
139. Koniakhin S V, Nalitov A V *Phys. Rev. B* **94** 125403 (2016)
140. Eidelman E D *Semiconductors* **51** 906 (2017); *Fiz. Tekh. Poluprovodn.* **51** 944 (2017)
141. Khalatnikov I M *Zh. Eksp. Teor. Fiz.* **22** 687 (1952)
142. Pollack G L *Rev. Mod. Phys.* **41** 48 (1969)
143. Challis L J *J. Phys. C* **7** 481 (1974)
144. Swartz E T, Pohl R O *Appl. Phys. Lett.* **51** 2200 (1987)
145. Stoner R J, Maris H J *Phys. Rev. B* **48** 16373 (1993)
146. Huberman M L, Overhauser A W *Phys. Rev. B* **50** 2865 (1994)
147. Mahan G D *Phys. Rev. B* **79** 075408 (2009)
148. Zhang L et al. *Phys. Rev. B* **83** 064303 (2011)
149. Meilakhs A P, Eidelman E D *JETP Lett.* **97** 38 (2013); *Pis'ma Zh. Eksp. Teor. Fiz.* **97** 42 (2013)
150. Meilakhs A P, Eidelman E D *JETP Lett.* **100** 81 (2014); *Pis'ma Zh. Eksp. Teor. Fiz.* **100** 89 (2014)
151. Landau L D, Lifshitz E M *Statistical Physics* Pt. 1 (Oxford: Pergamon Press, 1980); Translated from Russian: *Statisticheskaya Fizika* Pt. 1, 6th ed., ster. (Moscow: Nauka, 2018)
152. Landau L D, Lifshitz E M *Theory of Elasticity* (Oxford: Pergamon Press, 1986); Translated from Russian: *Teoriya Uprugosti* 6th ed. (Moscow: Nauka, 2007)
153. Ginzburg V L, Shabanskii V P *Dokl. Akad. Nauk SSSR* **100** 445 (1955)
154. Kaganov M I, Lifshits I M, Tanatarov L V *Sov. Phys. JETP* **4** 173 (1956); *Zh. Eksp. Teor. Fiz.* **31** 232 (1956)
155. Kogan Sh M *Sov. Phys. Solid State* **4** (10) 172 (1962); *Fiz. Tverd. Tela* **4** 2474 (1962)
156. Aronov A G, Ioselevich A S *Sov. Phys. JETP* **54** 974 (1981); *Zh. Eksp. Teor. Fiz.* **81** 1839 (1981)
157. Tian Z, Esfarjani K, Chen G *Phys. Rev. B* **86** 235304 (2012)
158. Abyzov A M, Kidalov S V, Shakhov F M *Phys. Solid State* **54** 210 (2012); *Fiz. Tverd. Tela* **54** 196 (2012)
159. Lyeo H-K, Cahill D G *Phys. Rev. B* **73** 144301 (2006)
160. Costescu R M, Wall M A, Cahill D G *Phys. Rev. B* **67** 054302 (2003)
161. Karr B W et al. *Phys. Rev. B* **61** 16137 (2000)
162. Taylor R E, Morreale J *J. Am. Ceram. Soc.* **47** (2) 69 (1964)
163. Meng W J, Eesley G L *Thin Solid Films* **271** 108 (1995)
164. Patsalas P, Logothetidis S *J. Appl. Phys.* **90** 4725 (2001)
165. Andrievsky R A, Dashevsky Z M, Kalinnikov G V *Tech. Phys. Lett.* **30** 11 (2004); *Pis'ma Zh. Tekh. Fiz.* **30** 22 (2004)
166. van den Brink A M, Dekker H *Phys. Rev. B* **51** 17842 (1995)
167. Babenko A Yu, Dideykin A T, Eidelman E D *Phys. Solid State* **51** 435 (2009); *Fiz. Tverd. Tela* **51** 410 (2009)
168. Zhao L-D et al. *Nature* **508** 373 (2014)
169. Novikov S V, Burkov A T, Schumann J *J. Electron. Mater.* **43** 2420 (2014)
170. Heremans J P *Nature* **508** 327 (2014)
171. Bhattacharyya S et al. *Nat. Mater.* **5** 19 (2006)
172. Barnard A S, Sternberg M *J. Mater. Chem.* **17** 4811 (2007)
173. Eidelman E D, Meilakhs A P *Nanosyst. Phys. Chem. Math.* **7** 919 (2016)
174. Eidelman E D et al. *J. Phys. D* **50** 464007 (2017)
175. Zavaritskii N *Sov. Phys. JETP* **48** 942 (1978); *Zh. Eksp. Teor. Fiz.* **75** 1873 (1978)
176. Kidalov S V, Shakhov F M, Vul A Ya *Diamond Relat. Mater.* **17** 844 (2008)

177. Shakouri A, Zebarjadi M, in *Thermal Nanosystems and Nanomaterials* (Topics in Applied Physics, Vol. 118, Ed. S Volz) (Heidelberg: Springer, 2009) p. 225
178. Snyder G J, Toberer E S *Nat. Mater.* **7** 105 (2008)
179. Majumdar A *Science* **303** 777 (2004)
180. Minnich A J et al. *Energy Environ. Sci.* **2** 466 (2009)
181. Harman T et al. *J. Electron. Mater.* **34** L19 (2005)
182. Heremans J P et al. *Thermoelectricity: Thermoelectric and Thermomagnetic Properties in Low Dimensional and Nanoscale Materials* (Berlin: Springer-Verlag, 2007)
183. Kajikawa T, in *Proc. of the 25th Intern. Conf. Thermoelectrics ICT2006* (Ed. P Rogl) (Vienna: IEEE, 2006) p. 93
184. Bottner H et al. *J. Microelectromech. Syst.* **13** 414 (2004)
185. Shakouri A *Proc. IEEE* **94** 1613 (2006)
186. Heremans J, in *Springer Handbook of Nanotechnology* (Ed. B Bhushan) (Berlin: Springer-Verlag, 2007) p. 345
187. Chen G *IEEE Trans. Compon. Packaging Technol.* **29** 238 (2006)
188. Koniakhin S V, Eidelman E D *Europhys. Lett.* **103** 37006 (2013)
189. Koniakhin S V, Eidelman E D *Nanosystems Phys. Chem. Math.* **5** 142 (2014)
190. Novoselov K S et al. *Nature* **490** 192 (2012)
191. Varlamov A A et al. *Phys. Usp.* **55** 1146 (2012); *Usp. Fiz. Nauk* **182** 1229 (2012)
192. Jiang J et al. *Phys. Rev. B* **72** 235408 (2005)
193. Mañes J L *Phys. Rev. B* **76** 045430 (2007)
194. Alofi A, Srivastava G P *J. Appl. Phys.* **112** 013517 (2012)
195. Klemens P G, Pedraza D F *Carbon* **32** 735 (1994)
196. Klemens P G *Theory of the a-Plane Thermal Conductivity of Graphite* (Ecklund, Science of Fullerenes and Carbon Nanotubes) (New York: Academic Press, 1995)
197. Tomchuk O V et al. *Diamond Relat. Mater.* **103** 107670 (2020)
198. Dideikin A T, Vul' A Y *Front. Phys.* **6** 149 (2019)
199. Dideykin A et al. *Diamond Relat. Mater.* **20** 105 (2011)
200. Nikolaeva M N et al. *Nanosystems Phys. Chem. Math.* **8** 665 (2017)
201. Kirilenko D A et al. *Micron* **68** 23 (2015)
202. Nikolaeva M N et al. *Russ. J. Appl. Chem.* **87** 1151 (2014); *Zh. Priklad. Khim.* **87** 1172 (2014)
203. Aleksenskii A E et al. *Tech. Phys.* **58** 1614 (2013); *Zh. Tekh. Fiz.* **83** (11) 67 (2013)
204. Koga T, Rabin O, Dresselhaus M S *Phys. Rev. B* **62** 16703 (2000)
205. Heremans J P et al. "Thermoelectric devices comprising a junction of dissimilar materials, i.e. exhibiting seebeck or Peltier effect with or without other thermoelectric effects or thermomagnetic effects; Processes or apparatus specially adapted for the manufacture or treatment thereof or of parts thereof; Details thereof", Patent US6670539, МПК H01L35/18, H01L35/34, H01L35/12, н 30.12.2000 Patents for H01L 35
206. Eidelman E D, Arkhipov A V *Phys. Usp.* **63** 648 (2020); *Usp. Fiz. Nauk* **190** 693 (2020)